N-bridged dimers of tetrapyrroles complexed by transition metals: syntheses, characterization methods, and uses as oxidation catalysts

Ümit İŞCİ[1], Fabienne DUMOULİN[1], Alexander B. SOROKİN[2,*], Vefa AHSEN[1,*]
[1]Gebze Institute of Technology, Department of Chemistry, P.O. Box 141 Gebze, 41400 Kocaeli, Turkey
[2]Institute of Researches on Catalysis and Environment in Lyon (IRCELYON), UMR5256 CNRS-University of Lyon 1, 2, av. A. Einstein, 69626 Villeurbanne Cedex, France

Abstract: N-bridged dimers of tetrapyrroles complexed by transition metals have been known for nearly four decades, and gained renewed attention when their powerful oxidation properties were recently evidenced. This article is a state of the art review of the reported complexes and of their synthetic methods. Beyond classical chemistry characterization tools, specific methods appropriate to their structure are used and are presented in detail. Finally, their uses and importance of oxidation catalysts are reviewed.

Key words: Tetrapyrrole, porphyrin, phthalocyanine, transition metal, N-bridged dimeric complexes, μ-nitrido, oxidation

1. Introduction

Tetrapyrrole derivatives are a large family of molecules, most of them being metalated and monomeric. The most common macrocycles, porphyrins and phthalocyanines, are related structures. Each of them have related properties, mainly electronic, conductive, redox, nonlinear, photophysical, or photochemical.[1−4] Tetrapyrroles are therefore versatile molecular materials exploited in various applications.[5,6] Since iron porphyrin complex constitutes active sites of many enzymes involved in the essential life processes of dioxygen transport, biosynthesis of hormones, detoxification of xenobiotics, and metabolism of pharmaceuticals, transition metal tetrapyrrole complexes have been intensively investigated as bioinspired catalysts. Porphyrin,[7] phthalocyanine,[8,9] corrole,[10] corrolazine,[11] and porphyrazine[12] complexes are efficient catalysts for many reactions.

Dimers formed of transition-metalated complexes of tetrapyrroles have a particular position in this type of molecule. Their formation and properties have been described by Ercolani and co-workers in 2003.[13] Several of their structural variation points are listed below:

- the nature of the tetrapyrrole ligand: porphyrin, phthalocyanine, or porphyrazine;

- the similarity or not of the two tetrapyrrole macrocycles: the dimeric complex can be homoleptic or heteroleptic, either because the two tetrapyyrole rings are of different nature or because they have different substitution patterns;

- the nature of the bridging atom: O (μ-oxo complex), N (μ-nitrido complex), or C (μ-carbido complex);

- the similarity or not of the two transition metal atoms complexing each tetrapyrrole macrocyle: iron is the most common but a few heterometallic complexes including one iron and one ruthenium or one manganese are reported as well.

---

*Correspondence: ahsen@gyte.edu.tr, alexander.sorokin@ircelyon.univ-lyon1.fr

Table 1. Structure of all reported complexes made of N-bridged dimers of tetrapyrroles. Below each structure is shown the molecule number, the two types of the two tetrapyrrole macrocycles (homoleptic or heteroleptic), the nature of the two transition metals (homometallic or heterometallic), and the related reference numbers.
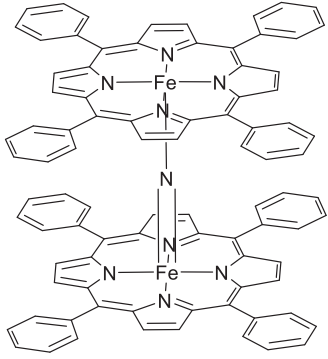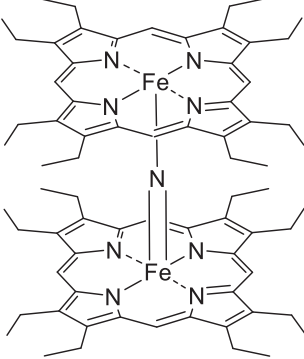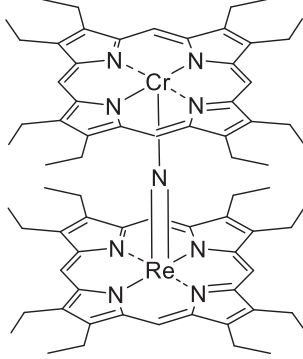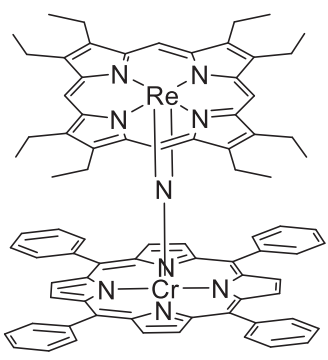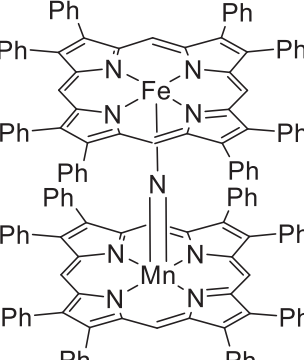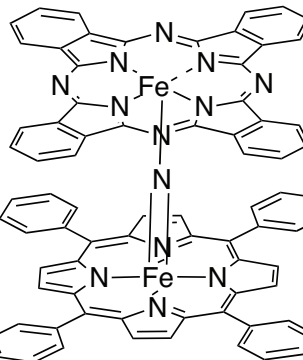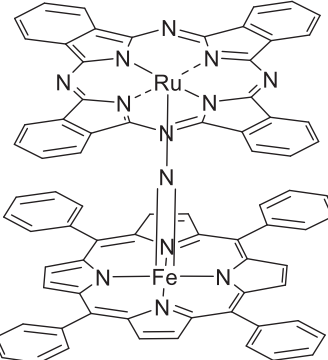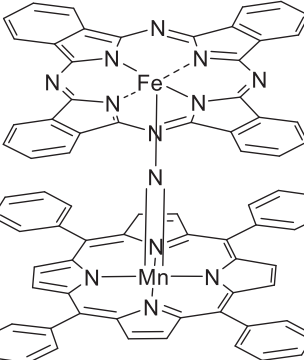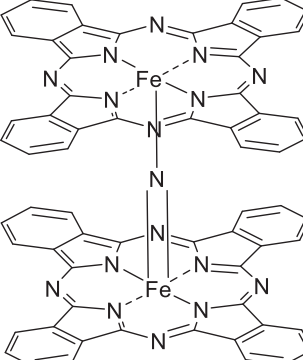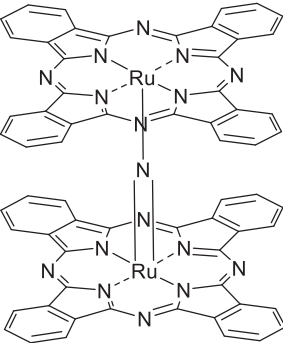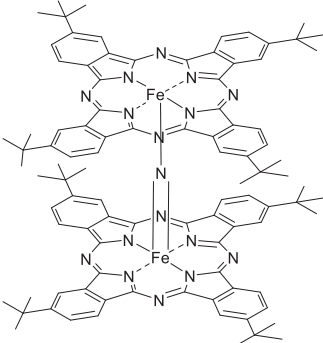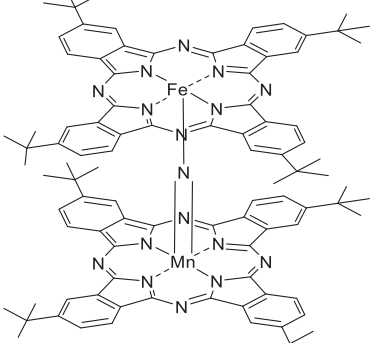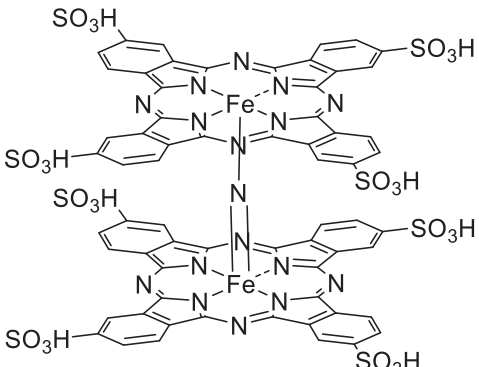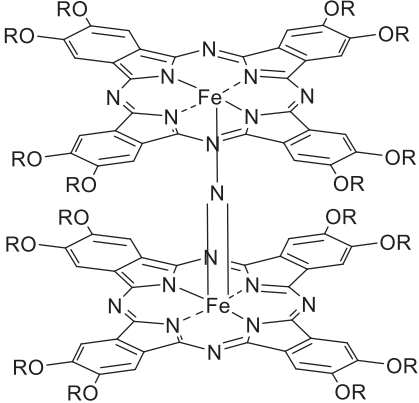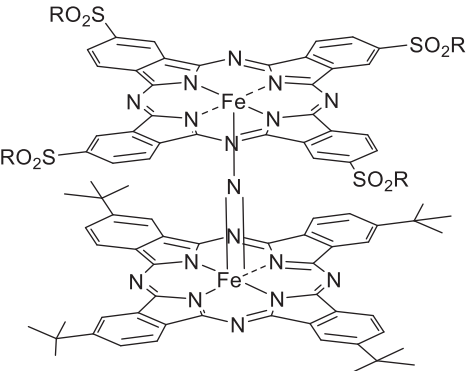

1 P-P homoleptic Fe-Fe homometallic Refs 14-22	**2** P-P homoleptic Fe-Fe homometallic Refs 23-24	**3** P-P homoleptic Re-Cr heterometallic Ref 25
4 P-P heteroleptic Re-Cr heterometallic Ref 25	**5** P-P homoleptic Fe-Mn heterometallic Ref 26	**6** P-Pc heteroleptic Fe-Fe homometallic Refs 27-28
7 P-Pc heteroleptic Fe-Ru heterometallic Ref 27	**8** P-Pc heteroleptic Fe-Mn heterometallic Refs 29-30	**9** Pc-Pc homoleptic Fe-Fe homometallic Refs 31-35

Table 1. Continued.

10
Pc-Pc homoleptic
Ru-Ru homometallic
Ref 36

11
Pc-Pc homoleptic
Fe-Fe homometallic
Refs 37-46

12
Pc-Pc homoleptic
Fe-Mn heterometallic
Ref 47

13-Me, **13-Et**, **13-tBu**, **13-nHex**,
13-cHex, **13-Ad**
Pc-Pc homoleptic
Fe-Fe homometallic
Refs 48-49

14
Pc-Pc homoleptic
Fe-Fe homometallic
Ref 50

15 (R: n-pentyl)
Pc-Pc homoleptic
Fe-Fe homometallic
Ref 51

16 (R: t-Bu)
Pc-Pc heteroleptic
Fe-Fe homometallic
Ref 52

This review will focus on μ-nitrido complexes. The structures of all the complexes reported so far are provided in Table 1. Twenty-one different complexes are reported. The synthetic accesses to these different complexes will be detailed, and the specific characterization means due to their particular structure will be explained. Finally, the use of these complexes as oxidation catalysts will be overviewed to evidence their properties and the need to investigate more deeply this category of molecules.
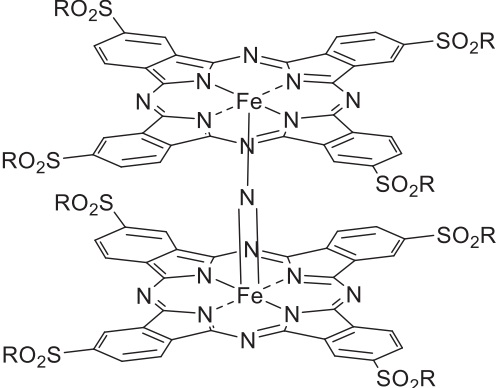
2. Synthesis

The preparation of μ-nitrido complexes is governed by the nature of the complex: homoleptic-homometallic, homoleptic-heterometallic, heteroleptic-homometallic, or heteroleptic-heterometallic. Two main trends for their synthesis is either the direct reaction of one or two tetrapyrrole macrocycles in the presence of sodium azide, or the preparation of a tetrapyrrole complex of M–N$_3$ or M≡N and then a second reaction with an appropriately metalated second tetrapyrrole macrocycle.

2.1. Preparation of homoleptic homometallic complexes

This type of complex is the most common, with two-thirds of the reported complexes being of this type. Except the sole example of compound **10** made of two Ru phthalocyanines, all the homometallic homoleptic complexes include two Fe atoms. When the tetrapyrrole is a porphyrin ring (compounds **1** and **2**), Fe porphyrin is initially converted into its Fe–N$_3$ derivative, which is isolated (Scheme 1a). Two Fe–N$_3$ porphyrins can react with each other by thermal decomposition leading to the corresponding μ-nitrido complex (Scheme 1b). So far, this synthesis has been applied only to Fe tetraphenylporphyrin (TPP)[14] and to Fe octaethylporphyrin (OEP).[23]
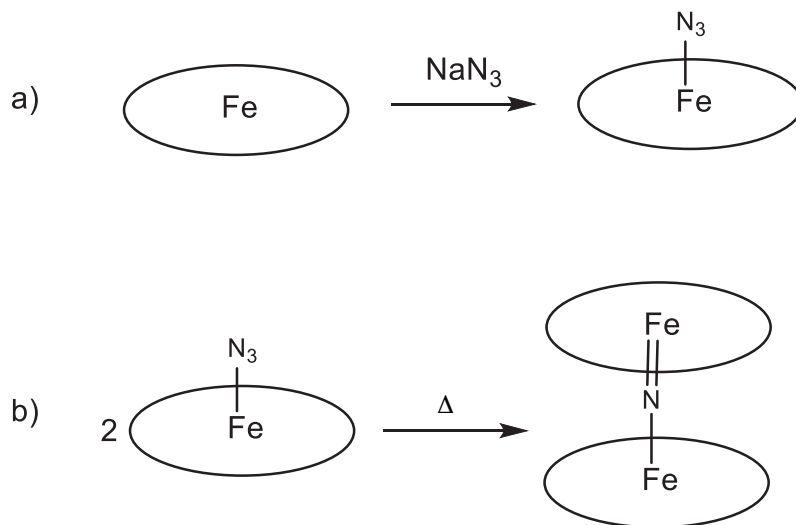
Scheme 1. Preparation of homometallic homoleptic complexes of porphyrins. In this scheme, ⬭ = porphyrin.

When the tetrapyrrole is a phthalocyanine ring, two appropriately metalated macrocycles react directly with sodium azide (Scheme 2), in yields around 50%–60%. Depending on the solubility of the monomeric precursor, α-chloronaphthalene or xylene can be used as the solvent.

The possibility to obtain N-bridged dimeric complexes of tetrapyrroles by the thermal decomposition of corresponding O-bridged complex in the presence of sodium azide is briefly evoked[32] but has not been really applied in the following reports.
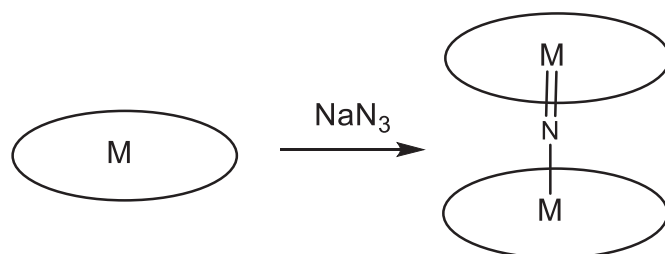
Scheme 2. Preparation of homometallic homoleptic complexes of phthalocyanines. In this scheme, ⬭ = phthalocyanine. M: Fe or Ru.

2.2. Preparation of homoleptic heterometallic complexes

Three homoleptic heterometallic complexes have been described: compounds **3**, **5**, and **12**.

Complex **3**, which consists of two OEP macrocycles, is prepared from ReOEP converted into Re≡N, which reacts afterwards with CrOEP.

In the case of **5** and **12**, which are both Fe-N-Mn (**5** is made of two OEP macrocycles and **12** of two ^{t}BuPcs), the Mn-metalated tetrapyrrole macrocycle is first of all converted into its Mn-N$_3$ derivative, which reacts afterwards respectively with FeOEP or Fe^{t}BuPc.

2.3. Preparation of heteroleptic heterometallic complexes

Three heteroleptic heterometallic complexes are described: compounds **4**, **7**, and **8**. Complex **4** consists of two different porphyrins: one TPP macrocycle complexing a Cr atom, and one OEP complexing a Re atom. As for complex **3**, the ReOEP is first of all activated into its Re≡N form and then reacts with CrTPP. Complexes **7** and **8** both consist of one TPP and one unsubstituted phthalocyanine macrocycle. The metalated TPP is firstly activated, respectively, into its Fe–N$_3$ form and into its Mn–N$_3$ form. These N$_3$-activated forms react then with the appropriately metalated phthalocyanine, respectively RuPc and FePc, leading to **7** and **8**.

2.4. Preparation of heteroleptic homometallic complexes

This category consists only of two compounds, complexes **6** and **16**, both with an Fe atom at the metal sites.

Complex **6** is made of one porphyrin and one phthalocyanine. The FeTPP is first converted into its Fe–N$_3$ derivative, which reacts with unsubstituted Fe phthalocyanine to give **6**.

Complex **16** consists of two phthalocyanines with different substitution patterns. It was prepared via a statistical mixture of the two starting Fe monomeric phthalocyanines, using a significant excess (10-fold) of one of the phthalocyanines allowed to obtain only two of the three possible complexes. Chromatographic separation led to complex **16** in 60% yield.

3. Characterization

The structural and electronic properties of μ-nitrido dimers can be investigated by a number of spectroscopic techniques. It is important to use several methods to fully characterize the complexes in terms of their structure, the oxidation and spin states of the metal centers, and the state of the supporting macrocyclic ligands. Many advanced spectroscopic techniques have been developed and used to understand the electronic structures of μ-nitrido dimers and even to study their chemical reactivity. UV-Vis, EPR, Mössbauer, XANES, and EXAFS methods can be used to determine the structures of the complexes and to understand which

structural parameters are important for the catalytic activity. The structural and spectroscopic data on μ-nitrido binuclear metal macrocyclic complexes described in the early literature were thoroughly reviewed by Ercolani and co-workers in 2003.[13] Herein, we discuss recent data and experimental approaches to detailed investigation of these complexes. Selected examples demonstrating the application of modern spectroscopic techniques are also provided.

3.1. Mass spectrometry

The identity of binuclear complexes can be evidenced using mass spectrometry methods. Mass spectrometry has significantly advanced in the last decade to characterize catalytic intermediates by atmospheric pressure ionization techniques. In particular, electrospray ionization mass spectrometry (ESI-MS) in the positive mode seems to be especially useful because the electrospray ion source allows keeping intact labile compounds. μ-Nitrido diiron phthalocyanines and porphyrins exhibit strong molecular cluster peaks with no or very minor fragmentation owing to monomerization. In addition, ESI-MS performed at variable low temperatures, called cold spray ionization mass spectrometry (CSI-MS), allows detection and investigation of elusive catalytic intermediates. As a rule, these high-valent diiron species are very reactive and, consequently, very unstable.
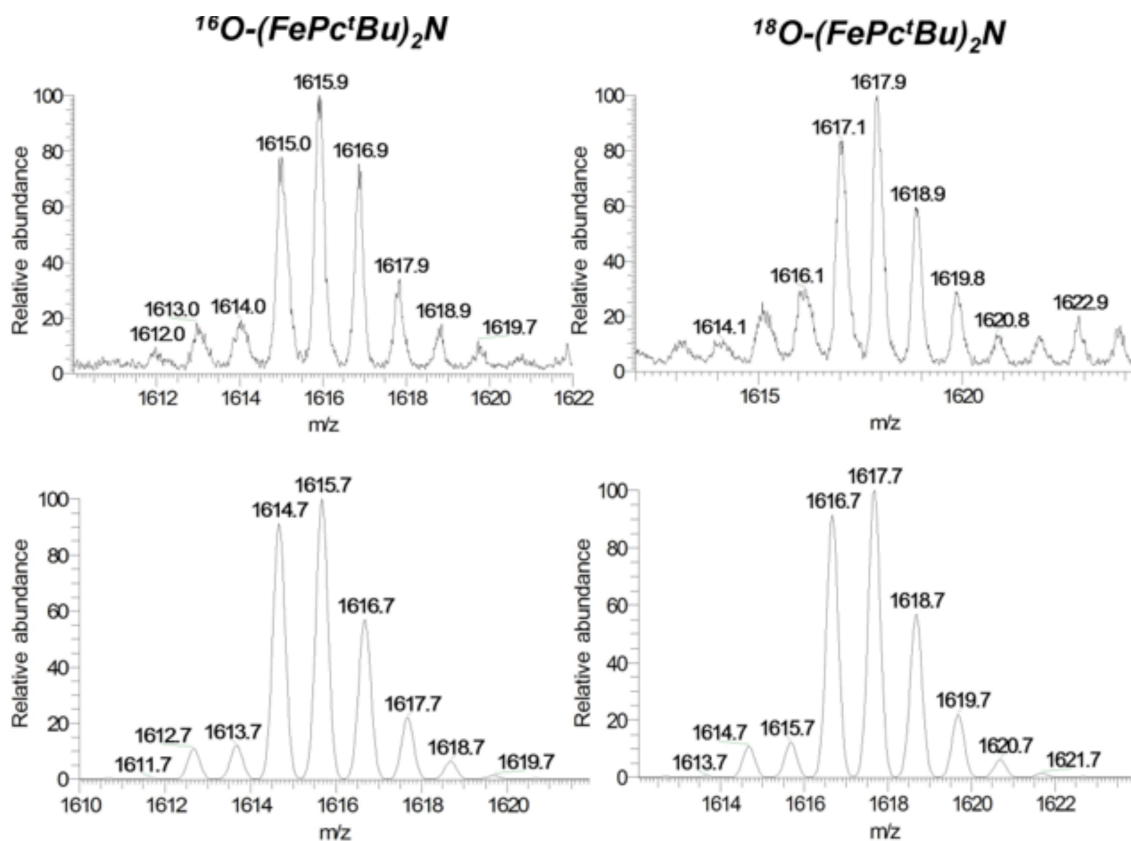
Figure 1. ESI-MS spectra of oxo-$(FePc^tBu_4)_2N$ prepared in the reaction between $(FePc^tBu_4)_2N$ and $H_2^{16}O_2$ or $H_2^{18}O_2$ (MeCN, 25 °C): isotope distribution patterns of the molecular peak cluster for ^{16}O-$(FePc^tBu_4)_2N$ (top left) and ^{18}O-$(FePc^tBu_4)_2N$ (top right), and simulated isotope distribution patterns for these species (bottom left and right, respectively).[37]

For this reason, very low temperatures and a freeze quenching approach are usually necessary to perform these studies. Highly sensitive mass spectrometry methods operating at low temperatures (–80 °C to 10 °C) are particularly suitable for detection and characterization of elusive short living active species.[53,54]

Thus, a very active μ-nitrido diiron oxo phthalocyanine involved in the oxidation of methane and other hydrocarbons was detected and investigated. The structure of this species was unambiguously confirmed by using ^{18}O isotope labeling (Figure 1, on the right).[37]

Along with a signal at m/z = 1599.8 of the parent $(FePc^{t}Bu_4)_2N$, a signal at $m/z = 1615.9$ corresponding to ^{16}O-$(FePc^{t}Bu_4)_2N$ was detected. When labeled $H_2^{18}O_2$ was used instead of $H_2^{16}O_2$ the signal of the molecular peak shifted for two units to $m/z = 1617.9$ due to formation of labeled ^{18}O-$(FePc^{t}Bu_4)_2N$ (Figure 1). Isotopic distribution patterns of the molecular peak in both cases, with $H_2^{16}O_2$ and $H_2^{18}O_2$, were identical with theoretical simulation distribution patterns.[37] The contribution of ESI-MS measurements in the rapid positive detection mode was essential for identification of the similar porphyrin diiron oxo species.[15]

Utilization of ESI-MS also evidenced the formation of the first high-valent complex on the mononuclear phthalocyanine platform.[55] While high-valent iron oxo species on porphyrin, corrole, and nonheme platforms have been prepared at low temperatures and characterized, the corresponding phthalocyanine species have often been postulated as active species, but have not been described until recently. For this experiment μ-nitrido complex was mixed with an m-chloroperbenzoic acid oxidant at –30 °C and the solution was analyzed directly by CSI-MS (Figure 2).
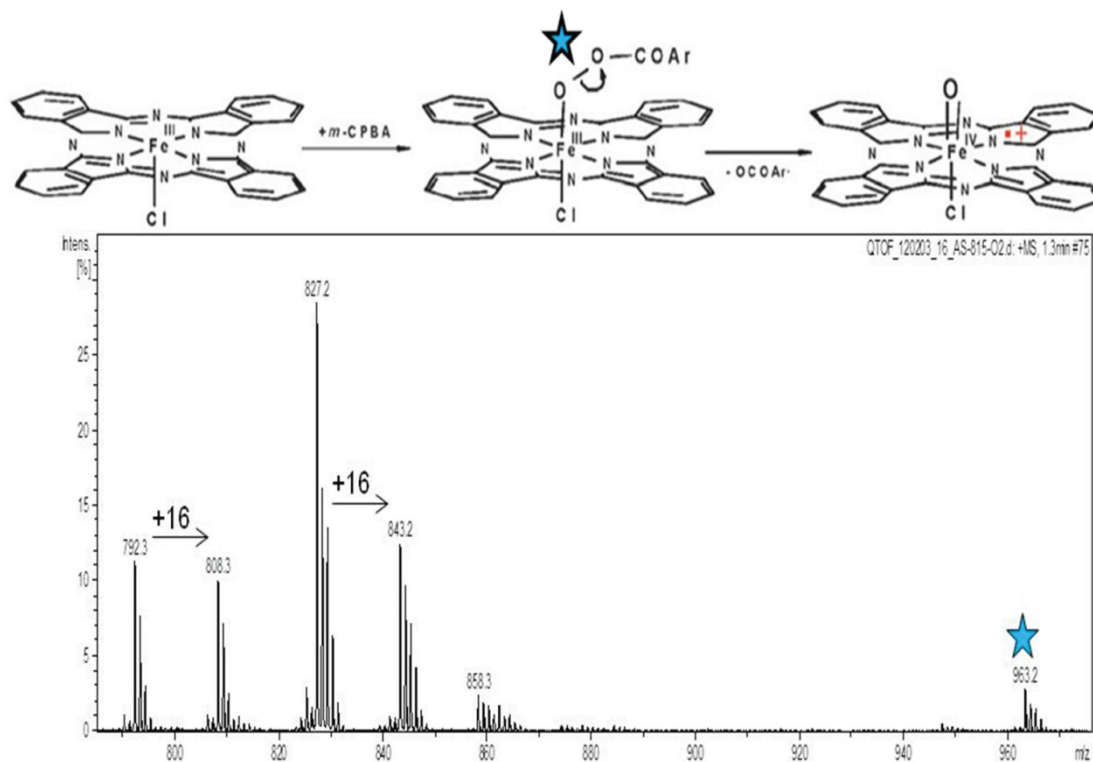
Figure 2. Preparation and CSI-MS characterization of the first high-valent iron oxo phthalocyanine complex and its peroxo precursor.

Along with the signal of the initial complex at $m/z = 792.3$ (for $[(Pc^tBu_4)Fe]^+$) a minor signal at $m/z = 963.2$ due to peroxocomplex $(Pc^tBu_4)Fe$-mCPBA was detected. Strong signals at $m/z = 808.3$ and $m/z = 843.2$ corresponding to $[(Pc^tBu_4)Fe=O]^+$ and $[(Pc^tBu_4)Fe=O(Cl)]^+$, respectively, were observed. The latter signal could result from oxo species after the loss of one electron under MS analysis conditions. The intensive signal at $m/z = 827.2$ can be due to $[(Pc^tBu_4)Fe=O(Cl) - O]^+$ fragmentation or due to initial $(Pc^tBu_4)FeCl$ complex after the loss of one electron under MS analysis conditions. The cryospray MS data suggested the mechanism of formation of the Fe(IV) oxo species and its formulation (Figure 2). Further evidence of the formation of the active oxo species was obtained by incubation of this species with labeled $H_2^{18}O$. A rapid isotopic exchange of the oxo ligand was observed, thus confirming the typical behavior of such oxo species (Figure 3).[56,57]
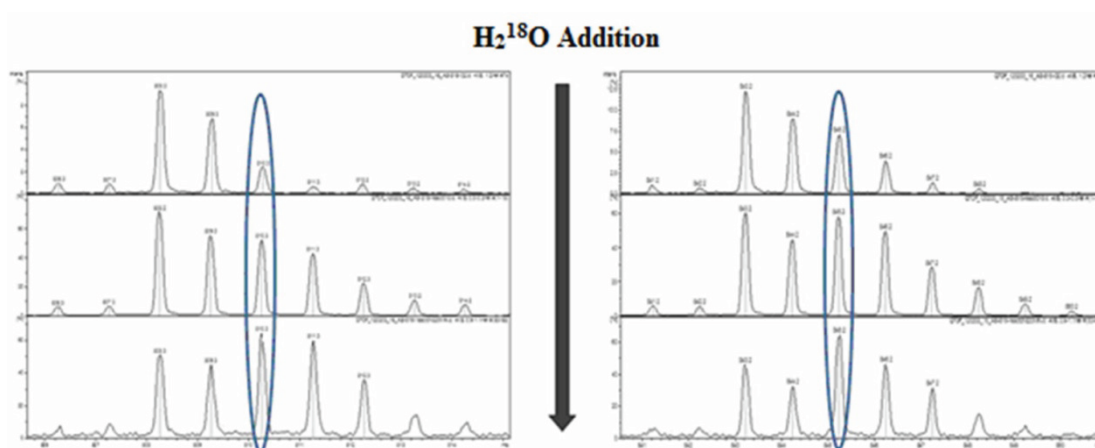
Figure 3. Positive CSI-MS spectrum of $[(Pc^tBu_4)Fe^{IV}=O(Cl)]^+$: experimental isotope distribution pattern of the $[(Pc^tBu_4)Fe^{IV}=O]^+$ molecular cluster peak and its evolution after addition of 40 μL of $H_2^{18}O$ per 1 mL of 10^{-6} M complex solution.

This example demonstrates the importance of the combination of the advanced mass spectrometry technique and isotopic labeling approach in obtaining valuable mechanistic data. Since the catalytic performance of the complexes is closely associated with the properties of the transient active species, the preparation and spectroscopic characterization of them is of great interest.

3.2. Structural characterization by X-ray diffraction analysis

In general, the structural information is determined by the preparation of crystals suitable for X-ray diffraction analysis (Figure 4). A relatively small number of X-ray structures of μ-nitrido dimeric macrocyclic complexes are available.[13] The most important structural data are collected in Table 2.

All the structures exhibit quite short Fe–Fe distances, between 3.25 and 3.36 Å, suggesting a strong $\pi - \pi$ interaction between aromatic macrocyclic rings. In general, the Fe–Fe distance is longer in μ-nitrido dimers based on tetraphenylporphyrin ligand because of the steric requirements of phenyl substituents. Out-of-plane deviation of iron atoms from the N4 plane is also more important for porphyrin complexes. Except eclipsed $[6(THF)H_2O]I_5$ and $[8(THF)H_2O]I_5$ structures, all structures are in staggered conformation with the twist angles between two macrocyclic rings from 23.1° to 39° (Table 2).
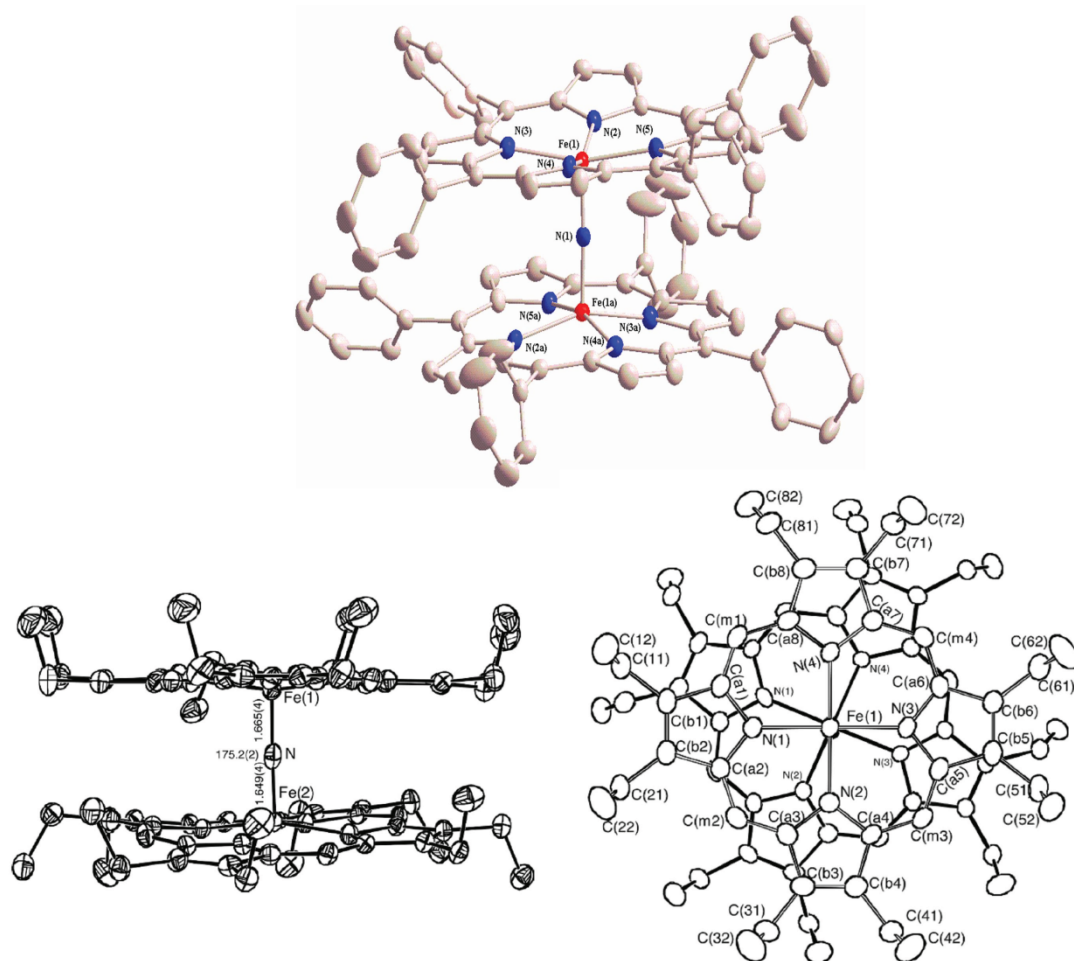
Figure 4. Crystal structure of μ-nitrido diiron tetraphenylporphyrin **1** (upper part)[21] and side-on and top-down view of μ-nitrido diiron octaethylporphyrin **2** (bottom part)[24]. Hydrogen atoms are omitted for clarity.

Table 2. X-ray structural data for the μ-nitrido metal phthalocyanine and porphyrin complexes. Bond lengths are given in Å.

Complex	M–N–M angle	M–N$_{bridge}$	M–M distance	Interplane distance	M–N$_{pyrrole}$	M–axial ligand	Staggering angle	Ref.
1	180.0°	1.6605(7)	3.32	4.15	1.991(3)	-	31.7°	16
1	177.0(4)°	1.6795(4)	3.36	3.93	2.003(3)	-	28.7°	21
2	175.2(2)°	1.657(11)	3.31	3.83	2.005(5)	-	23.1°	24
$[\mathbf{1}]^+(SbCl_6)^-$	180°	1.6280(7)	3.26	4.00	1.979(5)		30.3°	20
$[\mathbf{6}(THF)H_2O]I_5$	179.0(6)°	1.625(2) 1.655(2)	3.28	3.51	2.00(5)		eclipsed	27
$[\mathbf{8}(THF)H_2O]I_5$	178.6(7)°	Mn:1.669(12) Fe: 1.683(12)	3.35	3.59	2.018(11) 1.972(11)		eclipsed	30
$[\mathbf{9}]^{2+}$ Br$_2$	180°	1.639(2)	3.28	3.28	1.945(9)	2.495	39°	35
$[\mathbf{9}]$ (N$_3$)$_2$ I$_3$	177.4(4)°	1.650(1)	3.30	3.46	1.947(5)	2.152(7)	38.5(5)°	58

3.3. Structural characterization by extended X-ray absorption fine structure (EXAFS)

When single crystals suitable for X-ray diffraction analysis cannot be prepared the structural information can be obtained by EXAFS technique. In particular, this is the case for monomeric tetrasubstituted phthalocyanine complexes, which contain four positional isomers C_S, $C_{2\nu}$, C_{4h}, and D_{2h} with statistical ratio 4:2:1:1 given that the bulkiness of substituents does not disturb this ratio in favor of less sterically crowded positional isomers. Tetrasubstituted phthalocyanine complexes are difficult to separate and isolate in individual state. The preparation of crystals is therefore compromised and these complexes cannot be analyzed by X-ray diffraction.

In the case of μ-nitrido dimeric complexes on the tetrasubstituted phthalocyanine platform the situation is even worse because of the presence of 10 positional isomers. Nevertheless, the structural information on the first and second coordination spheres can be obtained by X-ray absorption spectroscopy using synchrotron radiation, namely by EXAFS.

The EXAFS structures of **11** and their dihalogenated derivatives$(Cl)(Pc^tBu_4)Fe^{IV}$–N–$Fe^{IV}(Pc^tBu_4)^{+\cdot}$·(Cl) (**11b**) and $(Br)(Pc^tBu_4)Fe^{IV}$–N–$Fe^{IV}(Pc^tBu_4)^{+\cdot}$·(Br) (**11c**) have been determined and are presented in Figure 5.[40]

	11	**11b**	**11c**
Fe - N_{bridge}	1.65 Å	1.68 Å	1.69 Å
Fe - $N_{pyrrole}$	1.94 Å	1.94 Å	1.93 Å
Fe - N_{meso}	3.41 Å	3.42 Å	3.45 Å
Fe - Fe distance	3.33 Å	3.35 Å	3.39 Å
Fe - Hal		2.33 Å	2.54 Å
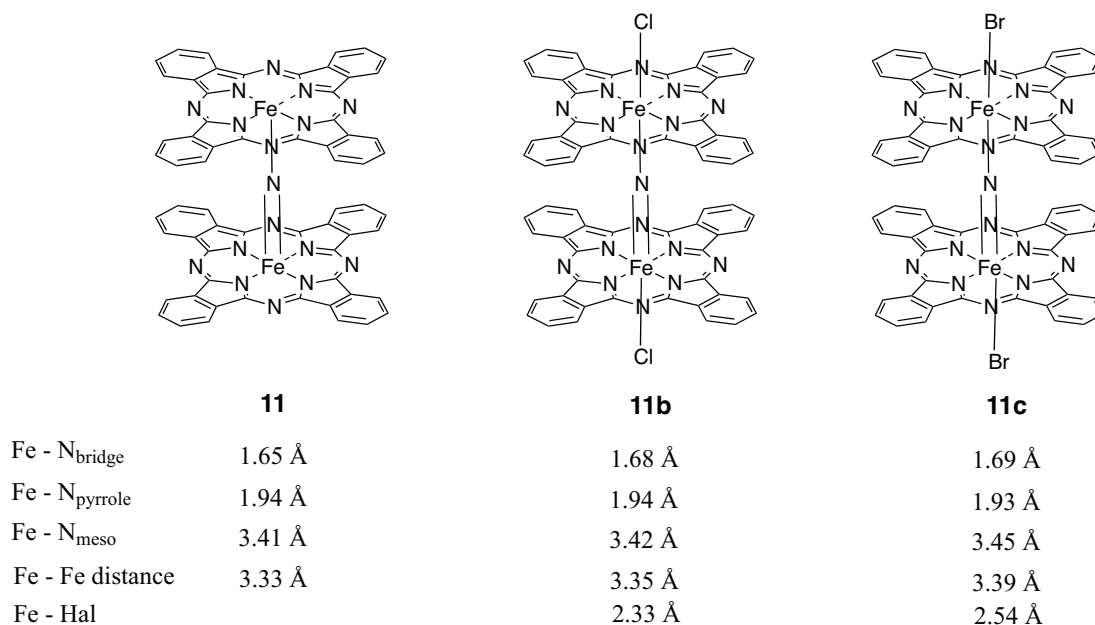
Figure 5. The structures of **11** and their dihalogenated derivatives **11b** and **11c** with quasi-linear Fe–N–Fe units determined by EXAFS. t-Butyl substituents are omitted for clarity.

The EXAFS spectra of **11**, **11b**, and **11c** are quite similar and differ from that of monomeric FePc$^tBu_4$, indicating the retention of a dimeric structure in **11b** and **11c**. The fragment Fe–N–Fe is quasi-linear, but iron sites are situated slightly out of the phthalocyanine plane, ca. 0.2 Å. The distance between two iron sites in **11** is quite short, 3.33 Å, suggesting a significant $\pi - \pi$ interaction of aromatic macrocyclic systems. Quite similar structural parameters were obtained for the complexes **13** bearing alkylsulfonyl substituents.[48,49] Upon an increase in iron oxidation state from Fe(+3.5)Fe(+3.5) in **11** to Fe(IV)Fe(IV) in **11b** and **11c** and axial coordination of halogen anions, small changes in bond distances occurred. Coordinated with halogen anions, iron atoms get closer to the macrocyclic plane and the Fe–N distance progressively increases from 1.65 Å in

11 to 1.69 Å in **11c**. Consequently, the Fe–Fe distance is also increased despite the increase in the Fe–N bond order from 3.33 Å to 3.39 Å. The lengths of Fe–Cl and Fe–Br bonds are 2.33 and 2.54 Å, respectively.[40]

However, the EXAFS study cannot address some essential structural features. For instance, the EXAFS approach cannot be used for the determination of the configuration (staggered or eclipsed) of the phthalocyanine planes of the dimer. It should be noted that this issue might be important in the determination of the spectroscopic properties of the μ-nitrido dimeric complexes. It is likely as well to affect the catalytic properties. For instance, UV-Vis and NMR studies of **15** revealed the existence of two different forms in apolar and polar solvents.[51] They differ in mutual orientation of two phthalocyanine planes. One rotamer was proposed to be close to eclipsed conformation and another one to staggered conformation.[51]

3.4. Determination of the oxidation state of metal sites: Mössbauer, XANES, and EPR spectroscopy

Information on metal oxidation state can be obtained by the combination of several spectroscopic methods. Mössbauer spectroscopy is a very efficient technique to characterize high valent iron complexes. Spectra are observed regardless of oxidation or spin state of the iron atoms (unlike EPR, where diamagnetic compounds are not detectable). Thus, from Mössbauer spectra one can determine the number of distinct Fe sites in the sample, their oxidation and spin state, and magnetic behavior. Diiron macrocyclic complexes can be analyzed in solution using freezing or directly after isolation of solid intermediates. Spectra of the catalysts in the conditions of catalysis and after catalytic tests can also be measured. However, the iron contents of the solutions and of the catalysts can be low to obtain Mössbauer spectra of the sufficient quality within reasonable experimental time. Consequently, ^{57}Fe enriched complexes should often be prepared and used for the catalyst preparations and characterization.

In the case of iron complexes, Mössbauer spectroscopy provides valuable information on the equivalence or nonequivalence of the iron sites and on their oxidation state. The measurements can be performed using regular iron complexes with natural abundance of ^{57}Fe of 2.119% (typically solid samples) or with specially prepared labeled ^{57}Fe complexes with more than 90% isotopic enrichment (typically frozen solutions). In the case of small iron content, an acquisition time of several days might be necessary to get Mössbauer spectra of good quality.

Only one doublet in the Mössbauer spectrum of **1** having formally Fe(III)(μ-N)Fe(IV) diporphyrin unit indicates the equivalent iron sites with an isomer shift and quadrupole splitting values of 0.18 and 1.08 mm s^{-1}, respectively.[13,59] Therefore, this structure can be described as Fe(+3.5)(μ-N)Fe(+3.5). The phthalocyanine μ-nitrido dimer **9** also contains equivalent Fe(+3.5) sites with $\delta = 0.06$ mm s^{-1} and $\Delta E_Q = 1.76$ mm s^{-1} at 77 K.[34] Interestingly, even heteroleptic complex **6**, TPPFe(μN)FePc, bears the same Fe(+3.5)(μ-N)Fe(+3.5) unit with Mössbauer parameters just between those of homoleptic **1** and **9**: $\delta = 0.113$ mm s^{-1} and $\Delta E_Q = 1.467$ mm s^{-1} at 77 K.[28] This means that the efficiency of the electronic exchange along the Fe–N–Fe fragment overcomes the effects produced by the different ligand environments around the two iron ions.[13] Although the Mössbauer technique can be applied only for iron complexes, it is very useful for determination of the metal oxidation states in heterometallic complexes. Heterometallic heteroleptic complex TPPFe(μN)RuPc (**7**) shows a single doublet with $\delta = 0.03$ mm s^{-1} and $\Delta E_Q = 0.90$ mm s^{-1}.[27] The lower value of the isomer shift than that measured in Fe(+3.5) complexes indicates Fe(IV) oxidation state and the complex **7** can be formulated as TPPFe^{IV}(μN)Ru^{III}Pc. In contrast to **7**, TPPMn(μN)FePc (**8**) exhibits $\delta = 0.19$ mm s^{-1} and $\Delta E_Q = 1.21$

mm s^{-1} values attributable to TPPMn^{IV}(μN)Fe^{III}Pc formulation.[29] The same Mn^{IV}(μN)Fe^{III} formulation has been attributed to homoleptic complex **12** with Pc^{t}Bu$_4$ ligand.[47] The oxidation states of Fe and Mn sites in **3** were not determined.[26]

On the basis of these data, one can suggest that in N-bridged dimers with different macrocyclic ligands, the charge delocalization between identical iron sites occurs through the bridging nitrogen atom.[13] In contrast, different metal centers in **7** and **8** lead to unequal localization of the charges to provide mixed-valence species.

The particular feature of the μ-nitrido macrocyclic platform is their capacity to stabilize high oxidation states of metal ions. Quite remarkably, a variety of high valent iron complexes containing Fe(IV)(μ-N)Fe(IV) unit have been prepared and characterized. In sharp contrast to bio-inspired high valent iron oxo species, many of these complexes are completely stable at room temperature. They can be readily identified using the Mössbauer technique due to very low and even negative values of isomer shift. Thus, Fe(IV)(μ-N)Fe(IV) dimers with porphyrin ligands exhibit δ values in the range from 0.03 to –0.13 mm s^{-1}, while Fe(IV)(μ-N)Fe(IV) phthalocyanine complexes show slightly more negative δ values.[13] For instance, the zero-field Mössbauer spectrum of (Cl)(Pc^{t}Bu$_4$)Fe^{IV}–N–Fe^{IV}(Pc^{t}Bu$_4$)$^{+\cdot}$(Cl) with two chloride anions coordinated in the axial positions of each iron site contained 1 doublet with δ = –0.10 mm s^{-1} and ΔE_Q = 1.64 mm s^{-1}, indicating identical Fe(IV) sites.[40]

$\mu-$Nitrido high valent diiron species can be also prepared by the treatment of the initial F(III)Fe(IV) complexes with H$_2$O$_2$ or m-chloroperbenzoic acid (m-CPBA).[21,37,38,44] It constitutes a special case, because these strong oxidizing entities bearing oxo in the axial position of one iron site, Fe^{IV}(μ-N)Fe^{IV}=O, are very active and hence very unstable. Their preparation and characterization should be performed under very low temperatures, typically between –60 °C and –90 °C. In addition, such short-living species cannot be isolated in the solid state owing to their instability. Consequently, to obtain spectra of sufficient quality ^{57}Fe-labeled complexes should be used. Finally, solvents containing heavy atoms should be avoided because of their absorption of γ-rays, which leads to a low signal-to-noise ratio and to spectra of low quality. Thus, dichloromethane, a chemically stable solvent with sufficiently low freezing temperature, widely used for oxidation and preparation of oxo species, is not an optimal solvent for Mössbauer measurements. For all these reasons, obtaining Mössbauer spectra of very active and short-living species is very challenging.

A significant achievement was the synthesis of the Fe^{IV}(μ-nitrido)Fe^{IV}=O tetraphenylporphyrin cation-radical species at –90 °C, which was characterized by UV-Vis, EPR, ESI-MS, and Mössbauer spectroscopies.[21] This oxo complex demonstrated a very high activity for oxygen atom transfer toward alkanes including methane. After addition of 5 equiv. m-CPBA at –90 °C the complex **1** with δ = 0.196 mm s^{-1} and ΔE_Q = 1.060 mm s^{-1} parameters was transformed to the species with δ = 0.00 mm s^{-1} and ΔE_Q = 0.746 mm s^{-1}. The strong decrease in the isomer shift value indicates an increase in iron oxidation state. The Mössbauer spectra recorded at 4.2 K under a 7 T external magnetic field indicated a zero spin density on both iron sites, i.e. a diamagnetic dinuclear core. The X-band EPR spectrum recorded on a frozen solution showed a single narrow symmetric line at g = 2.001 indicative of an organic radical. These observations strongly suggest this high valent diiron oxo species presents a well-isolated S = 1/2 ground state with the unpaired electron centered on a porphyrin moiety with no contribution of metal orbitals, which can only occur with two homovalent Fe ions of the same electronic spins and in strong antiferromagnetic interaction. Thus, detailed EPR and Mössbauer studies indicated that it comprises a strongly antiferromagnetically coupled Fe^{IV}(μ-N)Fe^{IV} stable unit behaving as a unique S_{FeFe} = 0 site weakly coupled to a porphyrin radical.[21]

EPR spectroscopy is a useful technique for determining electronic and magnetic properties of paramagnetic complexes. For studying iron species, EPR is quite a powerful method, since the parameters of spin Hamiltonian including g-factor and zero field splitting of Fe(III) low spin or high spin species strongly depend on the coordination state of iron and the eventual interaction (dimerization) of iron species. The earlier EPR spectra of mononuclear iron porphyrin complexes with various substituents demonstrated the possibility of distinguishing between the low-spin ferric species in the rhombic local symmetry and the high-spin ferric species in the tetragonal and rhombic symmetries. These species were found in different proportions at different temperatures, as well as in the compounds with various substituents. Due to antiferromagnetic interaction of two iron sites in Fe(III)Fe(IV) μ-nitrido dimeric complexes, their low spin state can be evidenced by EPR method. As for Fe(IV)Fe(IV) species, the presence of the cation-radical at supporting macrocyclic ligand (porphyrin or phthalocyanine) can be deduced from the presence of a narrow EPR signal at g $\sim$ 2. Therefore, the EPR investigations of diiron binuclear catalysts may provide important information about the structure of the active sites. Other useful information on the state of iron in the active species can be obtained by magnetic measurements and from XPS spectra.

The coordination of iron sites as well as iron oxidation state undergoes important changes in the catalytic cycle; therefore, the XANES and EXAFS spectroscopies could be especially useful for the characterization of active catalytic intermediates and often provide valuable data for understanding fine mechanistic details. An introduction to these techniques and their applications to resolving chemical problems can be found in some reviews.[60,61]

The local electronic structure of iron can be studied by analysis of the pre-edge region, which originates from the excitations of 1s electrons into the lowest unoccupied 3d electronic states. The K pre-edge feature of iron is sensitive to the oxidation state, the site symmetry, and the crystal field splittings.[62] The most useful parameters of the Fe–K pre-edge for determining Fe oxidation state and coordination number are the position of its maximum and the integrated intensity of the pre-edge peak.

The oxidation and spin states of iron atoms in series $[PcFe^{+3.5}NFe^{+3.5}Pc]^0$ (**9**), $[PcFe^{IV}NFe^{IV}Pc]^+PF_6$ (**9b**), and $[PcFe^{IV}NFe^{IV}(Pc^{\bullet+})]^{2+}Br_2$ (**9c**) have been studied by X-ray absorption spectroscopy and compared with those of monomeric PcFeCl.[42] The maximum position of the pre-edge peak in the XANES spectrum is around 7113.7 eV for Fe(III) (FePcCl), 7113.8 for Fe(3.5+) (**9**), and Fe(IV) (**9b**), whereas it shifted to 7114.7 eV for the Fe(IV) compound **9c**, indicating an increase in the iron oxidation state.

The pre-edge spectra of **11** and dihalogen derivatives $(Cl)(Pc^tBu_4)Fe^{IV}–N–Fe^{IV}(Pc^tBu_4)^{+\bullet}(Cl)$ (**11b**) and $(Br)(Pc^tBu_4)Fe^{IV}–N–Fe^{IV}(Pc^tBu_4)^{+\bullet}(Br)$ (**11c**) are presented in Figure 6 together with monomer FePc^{t}Bu reference.[40]

The XANES spectrum of monomeric FePc^{t}Bu has a small pre-edge peak at 7112.8 eV typical for octahedral or square-pyramidal Fe(III) complexes. Formation of μ-nitrido dimer **11** resulted in an increase in pre-edge intensity and shift of the pre-edge peak to higher energy 7114.1 eV. The increase in pre-edge intensity is consistent with oxidation of the iron centers because it increases the number of free d-orbitals and therefore the probability of 1s-3d electron transition. Shift of the pre-edge to higher energy is also consistent with the oxidation as it means an increase in the efficient positive charge on the iron central ion and consequently a stronger electron bonding.

Upon formation of dichloro- and dibromo complexes **11b** and **11c**, a further increase in pre-edge energy was detected (7115.2 eV for both **11b** and **11c**) and the second lobe of the pre-edge peak appears at 7113.4 eV (Figure 6). The increase in pre-edge energy reflects the higher oxidation state of iron with respect to that of **11**.

The appearance of two lobes in the XANES spectra of complexes **11b** and **11c** can probably be explained by the nonequivalent character of iron sites because of the presence of cation radical on one phthalocyanine ligand. It could lead to the removal of 3d orbitals degeneration and occurrence of multiple excited states, resulting in superposition of two types of pre-edges. It should be noted that the existence of the two-lobes feature of the pre-edge peak is a common feature of high valent Fe(IV)Fe(IV) dimers bearing cation-radical macrocyclic ligand. Thus, the high valent diiron complexes **11b** and **11c** can be formulated as $(Cl)(Pc^tBu_4)Fe^{IV}-N-Fe^{IV}(Pc^tBu_4)^{+\cdot}(Cl)$ and $(Br)(Pc^tBu_4)Fe^{IV}-N-Fe^{IV}(Pc^tBu_4)^{+\cdot}(Br)$, respectively.

Resonant inelastic X-ray scattering (RIXS) in Fe K-edge studies of these complexes can also be very fruitful to understand this exciting chemistry. RIXS gives a unique possibility to observe $3d^4$ spin systems, such as Fe^{IV}, which could possibly be transient species formed in the reaction of diiron complexes under oxidative conditions.[42] Dimeric iron complexes can be studied in pure form as well as grafted onto silica or other support with loadings of 0.1–0.5 wt % Fe. To protect unstable complexes from radiation damage the samples (pellets) should be measured in the sample holder cooled by liquid N_2. RIXS and EXAFS spectra can also be simulated theoretically and compared with the experimental data.

3.5. UV-Vis spectroscopy for the determination of the macrocyclic ligand state

As was discussed in the previous section, the presence of the cation-radical at the supporting macrocyclic ligand is attested by a narrow EPR signal at g $\sim$ 2. The typical EPR spectrum of a high-valent diiron phthalocyanine cation-radical complex is shown in Figure 7.[40] In addition, porphyrin cation-radicals exhibit a broad Q band in UV-Vis spectra between 600 and 650 nm. A typical example of the UV-Vis spectrum of the μ-nitrido diiron porphyrin cation-radical complex is shown in Figure 8.[21]
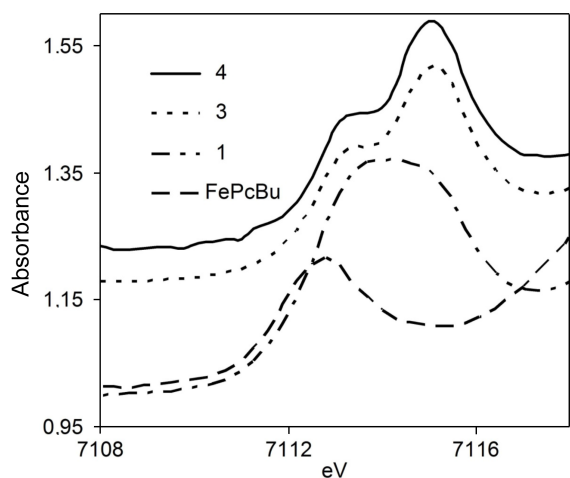
Figure 6. Pre-edge parts of the XAS spectra of monomeric $FePc^tBu$ (– – –), dimeric **11** (– • –), $(Cl)(Pc^tBu_4)Fe^{IV}-N-Fe^{IV}(Pc^tBu_4)^{+\cdot}(Cl)$ (**11b**) (—), and $(Br)(Pc^tBu_4)Fe^{IV}-N-Fe^{IV}(Pc^tBu_4)^{+\cdot}(Br)$ (solid line) (**11c**) complexes.
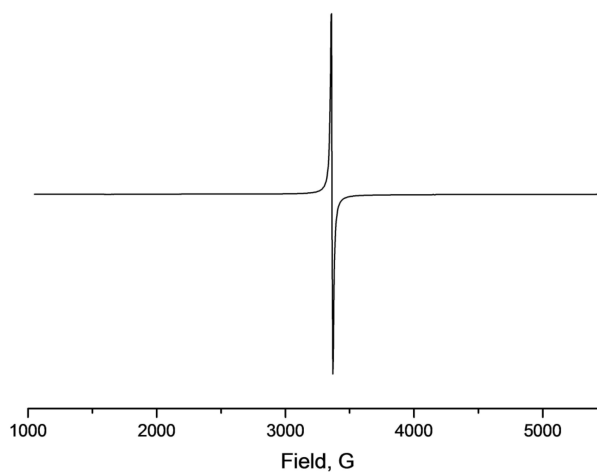
Figure 7. Solid state EPR spectrum of $(Cl)(Pc^tBu_4)Fe^{IV}-N-Fe^{IV}(Pc^tBu_4)^{+\cdot}(Cl)$ at 77 K.[40]

The formation of the high valent diiron complex on the phthalocyanine platform was evidenced by the appearance of broad bands in the regions 500–550 nm and 620–670 nm (Figure 9).[40,63,64]

Metal-centered one electron oxidation usually results in relatively small UV-Vis spectral changes.
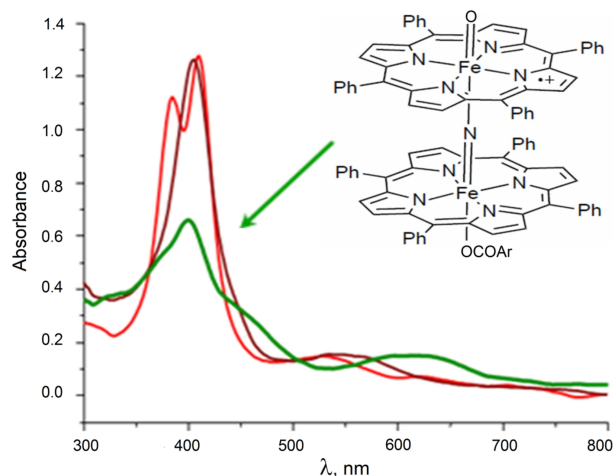
Figure 8. UV-Vis spectrum of the μ-nitrido high-valent diiron oxo species on tetraphenylporphyrin platform (green line) prepared by addition of m-chloroperbenzoic acid at –60 °C.[21] The broad Q band between 600 and 650 nm is indicative of the presence of porphyrin cation-radical.
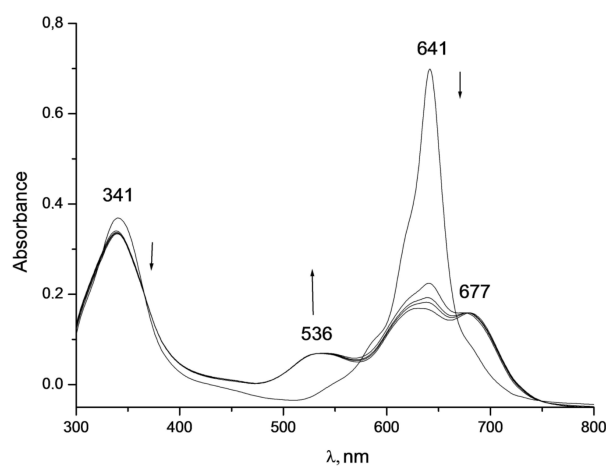
Figure 9. Spectral changes observed in the reaction of **11** with ^{t}BuOOH. Experimental conditions: CH_2Cl_2, [**11**] = 2.0×10^{-6} M, [^{t}BuOOH] = 0.015 M, 25 °C, spectra recorded after 3-min intervals.[40]

4. Catalytic oxidation

N-Bridged diiron phthalocyanine complexes as powerful oxidation catalysts have been used in oxidation reactions since 2008. Earlier, their μ-oxo diiron counterparts were also investigated in catalytic oxidation.[65−69]

Oxidation reactions using N-bridged diiron phthalocyanine catalysts will be explained in detail. The main oxidation substrates are alkanes (methane and propane), aromatics (benzene, toluene and p-xylene), cyclohexene and cyclohexane, chlorinated phenols, and thiols. The complexes were used either as homogeneous catalysts or on supporting heterogeneous systems.

Remarkably, μ-nitrido diiron complexes are much stronger oxidants compared to their mononuclear counterparts.[21]

4.1. Oxidation of light alkanes

One of the most difficult oxidation reactions is C–H bond oxidation.

The oxidation of methane is generally carried out at very high temperature and pressure[70−74] because of the very high C–H bond energy (435 kJ mol^{-1}) of methane. Using N-bridged diiron phthalocyanine **11** as catalyst, oxidation of methane was performed in mild conditions (Scheme 3).[37]

Scheme 3. Oxidation of methane by **11** using H_2O_2 as oxidant.

The oxidation of methane was conducted in CH_3CN at 40 °C. The main product was formic acid after careful studying by GC-MS. There were methanol, acetic acid, and acetone in the oxidation mixture, as well.

The same oxidation products could be obtained by oxidation of CH_3CN. Therefore, the oxidation reaction was performed in CD_3CN. It was observed that 68% of products originated from the oxidation of methane and 32% of products were obtained from the oxidation of acetonitrile (ratio 2:1). In order to overcome this problem, a silica supported μ-nitrido phthalocyanine dimer was prepared using dimer **11**, and the oxidation of methane was performed in water.[37]

The proposed oxidation mechanism is represented in Figure 10. The strong catalytic activity and stability of the **11**-SiO_2-H_2O_2 system were obtained in the presence of small amounts of acid. A very high performance was obtained in 0.075 M H_2SO_4 aqueous solution.[39,41] Oxidation products were obtained in high yield, reaching up to 92%. Remarkably, when the reaction was conducted in pure water, the complex was completely bleached after 20 h of reaction. The recovered supported catalyst after 20 h was still blue in diluted acid solution. Therefore, the stability of the complex was increased in the presence of acid.
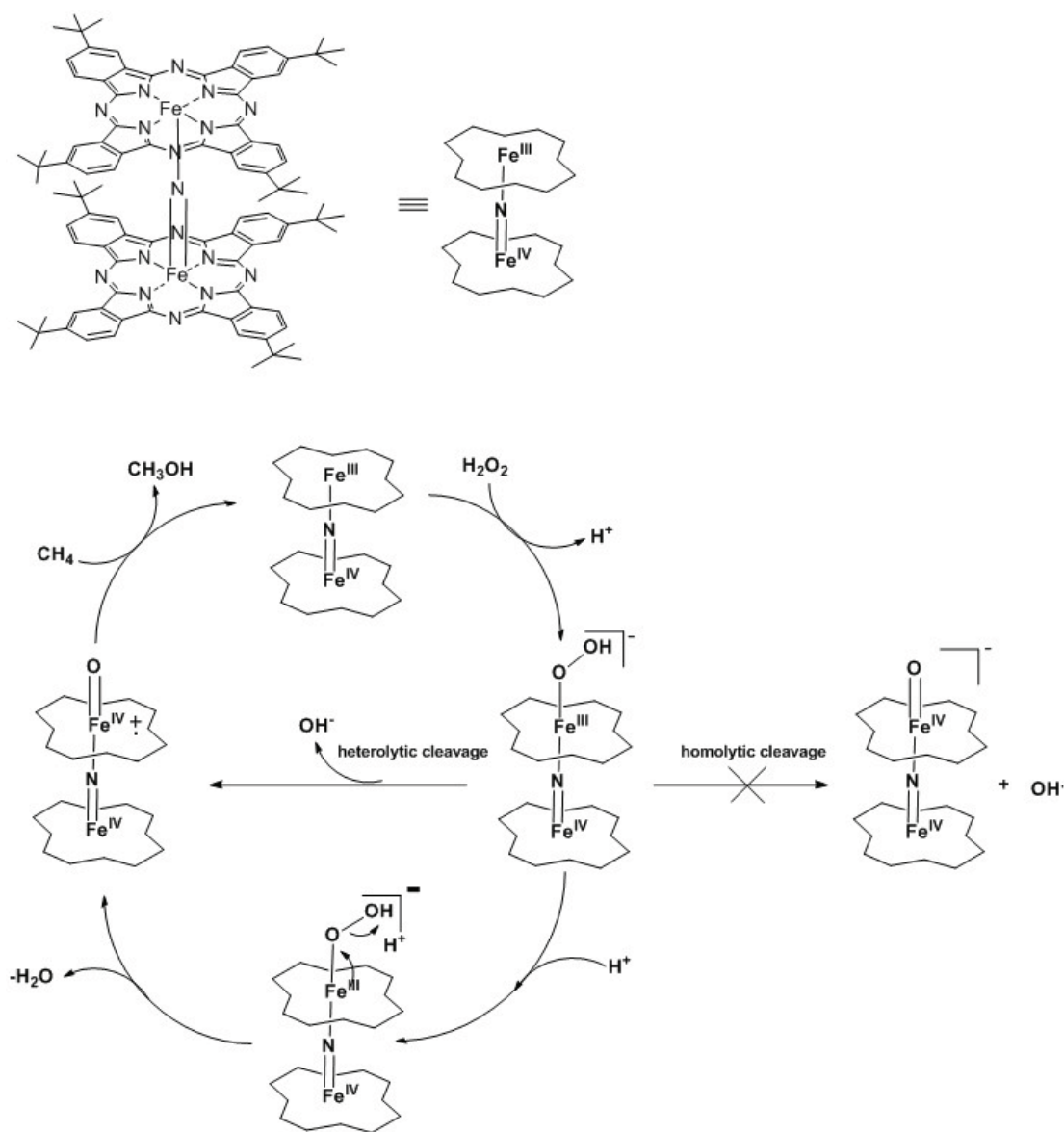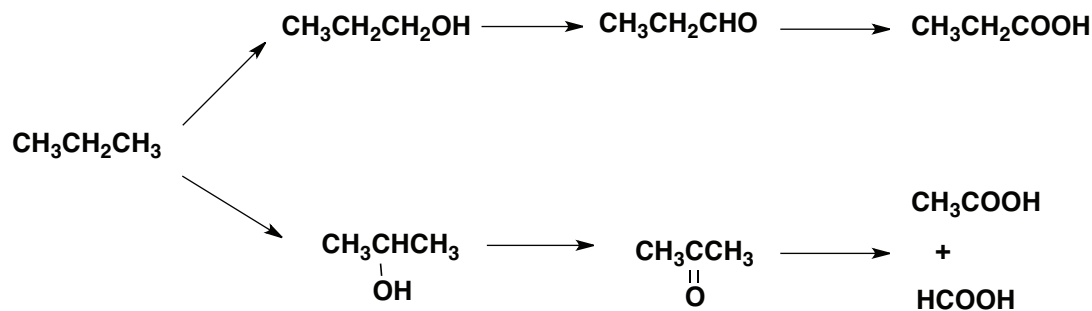

Figure 10. Proposed mechanism of the oxidation of methane.

The stability of the **11**-SiO_2 system and the oxidation product compositions were studied in detail under modified reaction conditions.[46] The oxidation reaction was performed in the presence of 5000 eq. of H_2O_2 with respect to the catalyst in pure water. The formation of CH_3OOH and CO_2 was analyzed using ^{1}H NMR and GC methods. There were two possible ways for free radical degradation of phthalocyanine complex and leaching of the iron ions to solution: (i) generation of OH radicals in the close locality of the absorbed complex catalyzed by silica support containing 20 ppm of iron and (ii) generation of OH radicals by **11**, which would lead to characteristic instability. The SiO_2 support bearing 20 ppm of Fe exhibited significant H_2O_2 decomposition.

The μ-nitrido diiron dimer **11**-H_2O_2 system can be used for the oxidation of other alkanes.[39] The catalytic oxidation of propane was performed in pure water. The solubility and concentration of propane in H_2O are lower than those of methane and a lower propane pressure (20 bars) can be applied. The oxidation of propane was quite efficient under these conditions. GC-MS analysis showed that the reaction mixture involved propan-1-ol, propan-2-ol, propionaldehyde, acetone, and propionic, acetic, and formic acids (Scheme 4).

$$CH_3CH_2CH_2OH \longrightarrow CH_3CH_2CHO \longrightarrow CH_3CH_2COOH$$

$$CH_3CH_2CH_3$$

$$CH_3CHCH_3 \longrightarrow CH_3CCH_3 \longrightarrow CH_3COOH + HCOOH$$
$$\quad\;\; OH \qquad\qquad\quad O$$

Scheme 4. Oxidation of propane.

Several oxidation products were obtained in the oxidation of propane, as alcohols, the primary reaction products, are more easily oxidized. This was confirmed using acetone as a substrate. The acetone was oxidized under these conditions with 84% conversion to form formic and acetic acids as major products.

4.2. Oxidation of aromatics

N-bridged diiron phthalocyanine complex **11** exhibited high activity for the mild oxidation of benzene.[38]

Turnover number based on PhOH reaches 66 cycles. The Fe–N–Fe structural unit of μ-nitrido diiron complex **11** is important for this catalytic activity (Figure 11). While monomeric iron phthalocyanine (FePc^{t}Bu$_4$) and μ-oxo (FePc^{t}Bu$_4$)$_2$O complex were quickly decomposed and were not catalytically active in the formation of benzene oxide during the oxidation of benzene, complex **11** exhibited the formation of benzene oxide (Table 3).

Table 3. Oxidation of PhH by H_2O_2 catalyzed by **11**.[a]

[PhH]/$_M$	T (°C)	t/h	Conversion (%)	TON$_{PhOH}$
0.1	20	48	14	11
0.1	40	20	20	12
1	40	20	n.d.[b]	28
5.57	60	24	n.d.	66
11.14[c]	60	4	n.d.	32

[a] Conditions: [x] = 2.4 × 10^{-4} M, [H_2O_2] = 0.22 M in two mL of CH_3CN. [b] n.d.: not determined. [c] Neat PhH
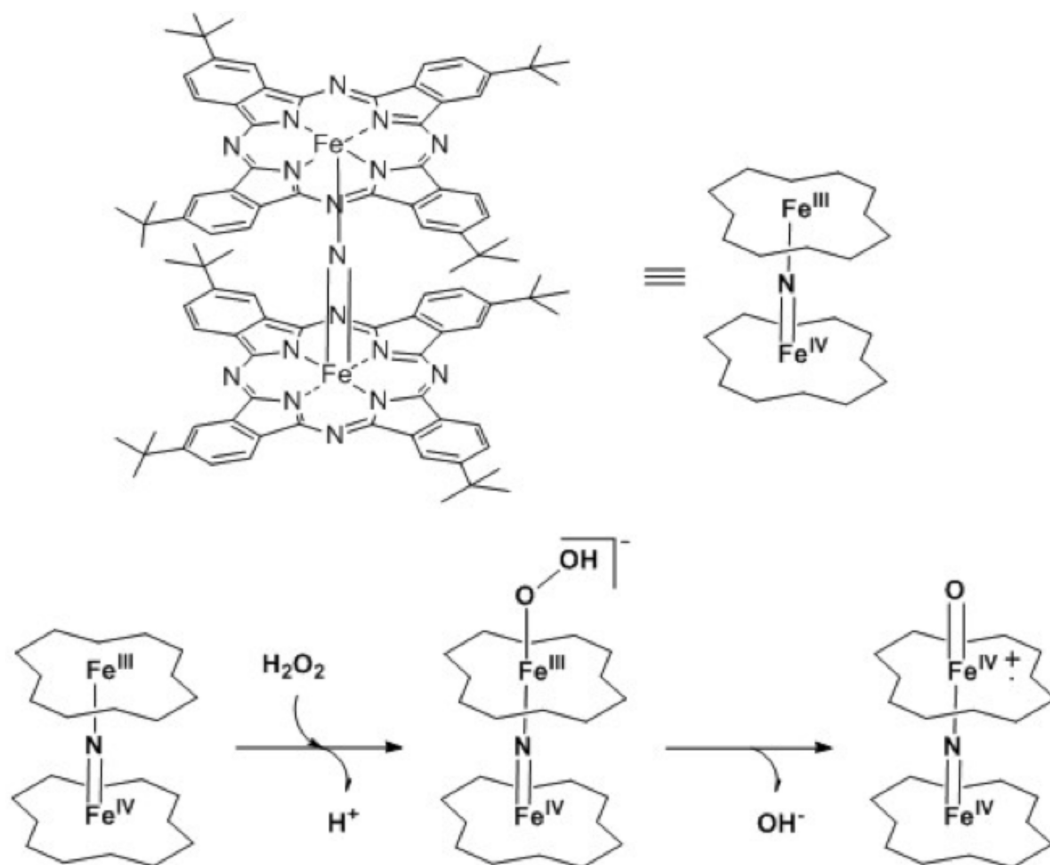
Figure 11. Proposed mechanism of the formation of high valent diiron oxo species.

The formation of benzene oxide in the **11**-H_2O_2 systems is compatible with the proposed mechanism. The use of 1,3,5-trideuterobenzene as a novel mechanistic probe is significant to check the amount of this phenomenon in the catalytic system. Only p-benzoquinone-d_2 can be formed without NIH shift (NIH is the acronym of the National Institutes of Health where the shift was evidenced). The product achieved in the oxidation of 1,3,5-trideuterobenzene by **11**-H_2O_2 contained 75% p-benzoquinone-d_2, 19% p-benzoquinone-d_3, and 6% p-benzoquinone-d_1, thus indicating an NIH shift.

Oxidation of alkyl aromatics such as toluene and p-xylene is one of the most important reactions in industrial chemistry.[75] These reactions are often performed with corrosive, toxic, or carcinogenic materials and with low selectivity. The composition of products obtained is dependent on the reaction conditions (catalyst, oxidizing agent, and solvent).

The catalytic properties of μ-nitrido diiron phthalocyanine complexes were tested in the industrially important oxidation of toluene (Scheme 5) and p-xylene (Scheme 6) by ^{t}BuOOH.[48]
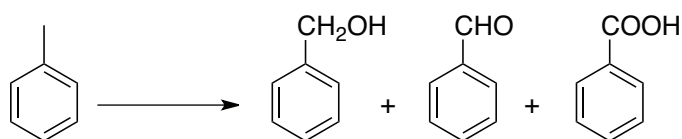
Scheme 5. Oxidation of toluene.

It was observed that μ-nitrido diiron complex **13-nHexyl** and **13-tBu** were efficient catalysts for oxidation of toluene. The catalytic system exhibits benzylic oxidation compared with aromatic oxidation. The main oxidation products were benzoic acid and benzaldehyde. The ratio of products was very similar for the two catalysts. Comparative experiments with μ-nitrido diiron complex **11** as catalyst for the oxidation of toluene showed the influence of the structure of the diiron N-bridged phthalocyanine on the catalytic properties. While **13**-nHexyl and **13-tBu** were quite selective to benzoic acid, up to 83%, **11** afforded benzaldehyde as the principal product with selectivity up to 51% (Table 4).

Table 4. Oxidation of toluene by TBHP catalyzed by **13-nHexyl** and **13-tBu**.

Catalyst	T (°C)	TON	Benzyl alcohol (%)	Benzaldehyde (%)	Benzoic acid (%)
13-nHexyl	20	92	6	21	73
	40	197	5	12	83
	60	167	6	13	81
13-tBu	20	59	7	20	73
	40	86	7	16	77
	60	115	7	16	77

Benzylic oxidation was also observed for the oxidation of p-xylene. The main products of benzylic oxidation were 4-methylbenzyl alcohol, p-tolualdehyde, and p-toluic acid. The oxidation of p-xylene also resulted in the products of benzylic oxidation: 4-methylbenzyl alcohol, p-tolualdehyde, and p-toluic acid (Scheme 6). Interestingly, both catalysts performed the selective oxidation of only one methyl group. Oxidation of both methyl groups was not observed. The products of aromatic oxidation were also absent.
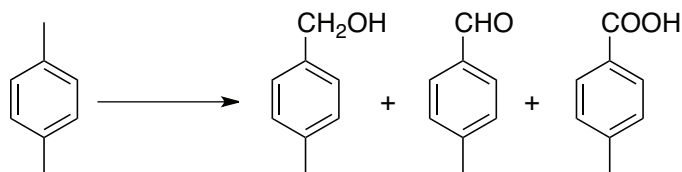
Scheme 6. Products of p-xylene oxidation.

While the oxidation of toluene in the presence of **13-nHexyl** was superior compared to **13-tBu** in terms of turnover numbers and selectivity to benzoic acid, **13-tBu** showed higher turnover numbers and selectivity than **13-nHexyl** in oxidation of p-xylene. A high performance was obtained at 60 °C with **13-tBu**: TON attained almost 600 catalytic cycles (Table 5).

**Table 5.** Oxidation of p-xylene by TBHP catalyzed by **13-nHexyl** and **13-tBu**

Catalyst	T (°C)	TON	4-Methylbenzyl alcohol (%)	p-Tolulaldehyde (%)	p-Toluic acid (%)
13-nHexyl	20	164	14	34	52
	40	291	15	25	60
	60	312	17	28	55
13-tBu	20	185	14	34	52
	40	339	13	22	65
	60	587	15	19	66

Finally, μ-nitrido diiron phthalocyanine complexes **13-nHexyl** and **13-tBu** performed the selective oxidation of only one methyl group. The results obtained for these industrially important oxidation reactions show the usefulness of μ-nitrido diiron phthalocyanine complexes as oxidation catalysts.

4.3. Oxidation of tetralin

$\mu-$Nitrido diiron phthalocyanine complex **11** was encapsulated with MIL-101 for the selective oxidation of tetralin into 1-tetralone, a diesel fuel additive and an intermediate for the synthesis of agricultural chemicals (Scheme 7).[76]

tetralin   1-tetralol   1-tetralone
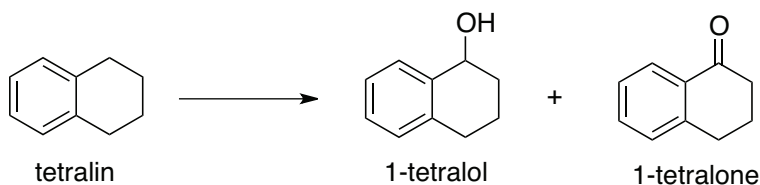
Scheme 7. Oxidation of tetralin.

The encapsulated μ-nitrido diiron phthalocyanine complex **11** was tested in oxidation of tetralin.[77] Different metal phthalocyanine catalysts in aerobic tetralin oxidation were used, in particular, two different perfluorinated complexes (MPcF16, M = Fe, Ru) and the bulky dimer **11**, which were selected for encapsulation. The activities and selectivities are presented in Table 6. μ-Nitrido diiron phthalocyanine complex **11** exhibited better catalytic activity than monomeric perfluorinated phthalocyanine complexes in homogeneous condition.

Table 6. Oxidation of tetralin using homogeneous catalysts.

		Complexes	
	11	FePcF$_{16}$	RuPcF$_{16}$
χ^a [%]	25	21	38
S$_{one}^b$ [%]	69	68	70
TON^c	7400	3400	5200

^{a} Conversion of tetralin. ^{b} Selectivity toward 1- tetralone. ^{c} Turnover number after 6 h for 1-tetralol and 1-tetralone.

The phthalocyanine-MOF materials were prepared by wet infiltration of the deep blue phthalocyanine solutions into Cr-MIL-101 with a maximal theoretical complex loading inside the MOF of 9 wt %. After slow evaporation of the solvent (acetone for perfluorinated phthalocyanine and CH_2Cl_2 for **11**, any complexes not strongly bound to the host MOFs were removed by washing until the filtrate remained colorless. These encapsulated heterogeneous complexes were tested in oxidation of tetralin. The activities and selectivities are presented in Table 7.

The encapsulation of metalated phthalocyanines in MIL-101 showed an activity increase of approximately one order of magnitude. This increase in activity may result from the dispersion of the molecular complexes as isolated monomers in the nanopore cavities and/or from the confinement effects provided by the host porous structure. In contrast, the **11** dimer, which is too large to penetrate into the porous structure, does not show this synergistic effect.

Table 7. N_2 physisorption results and catalytic performance of incorporated MPc@MIL-101 after 6 h and 24 h.

			Complexes	
Pc@MIL-101	MIL-101	11@MIL-101	FePcF$_{16}$@MIL-101^c	RuPcF$_{16}$@MIL-101
S$_{BET}^a$[m^2 g^{-1}]	2500	2450	2220	2120
V$_P^b$[cm^3 g^{-1}]	1.22	1.16	1.08	1.03
χ [%]	0/-	4/-	17/33	34/48
S$_{one}^d$ [%]	-/-	79/-	80/80	62/74
TON^e	0/-	5100/-	24,200/48,200	30,900/46,300
Size [nm × nm]	1.47 × 1.6^f	2.0 × 2.0^g	1.3 × 1.3^g	1.3 × 1.3^g

^{a}S$_{BET}$ at p/p0 = 0.05–0.2. ^{b}Total volume at p/p0 = 0.95. ^{c}Conversion of tetralin. ^{d}Selectivity toward 1-tetralone. ^{e}Turnover number after 6 h/24 h. ^{f}Hexagonal pore window of MIL-101. ^{g}Sizes of Pc complexes.

4.4. Oxidation of cyclohexene and cyclohexane

$\mu-$Nitrido diiron octaethylporphyrin complex **2** was used as catalyst in the oxidation of cyclohexane (Scheme 8) and cyclohexene (Scheme 9) by ^{t}BuOOH.[23]
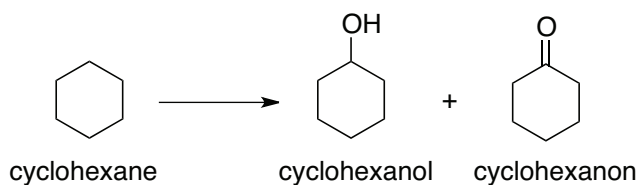
Scheme 8. Oxidation of cyclohexane.
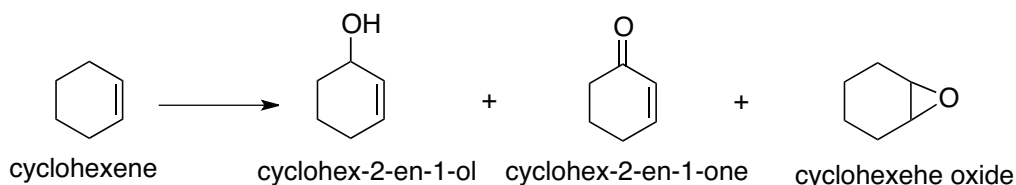
Scheme 9. Oxidation of cyclohexene.

The oxidation was performed in CH_3CN at 60 °C. Cyclohexanol and cyclohexanone were obtained as the main oxidation products of the oxidation of cyclohexane after 4 h.

The products of the oxidation of cyclohexene were cyclohex-2-en-1-one, cyclohex-2-en-1-ol, and cyclohexene oxide. The catalytic system was selective for the cyclohex-2-en-1-one (82%).

4.5. Oxidation of chlorinated phenols

Water-soluble μ-nitrido diiron phthalocyanine **14** was used as oxidation catalyst for the oxidative degradation of chlorinated phenols in water with hydrogen peroxide, an environmentally friendly oxidant.[78]

The complete conversion of 2,6-dichlorophenol was obtained using 0.5–1 mol % catalyst amounts with the total organic carbon removal up to 43% to form CO_2 and CO in 10:1 ratio (Schemes 10–12).
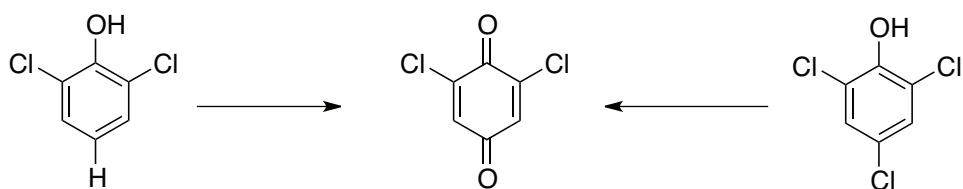
Scheme 10. Proposed first step of the oxidation of chlorinated phenols: formation of the quinone.
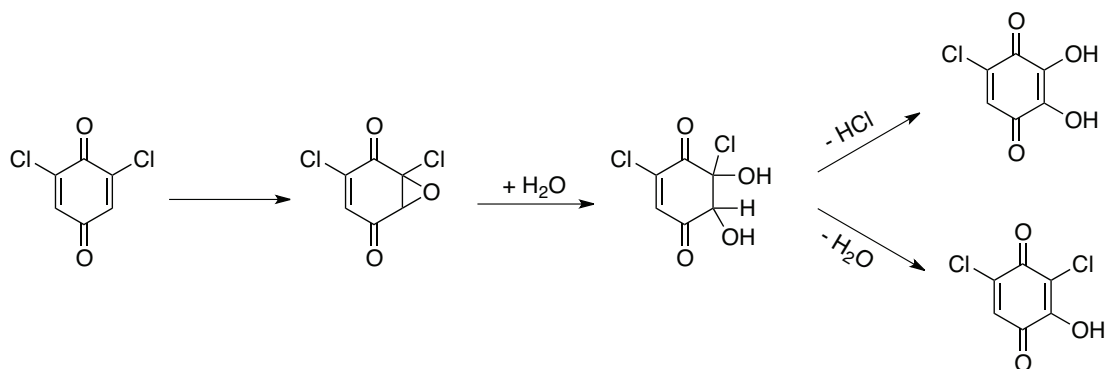
Scheme 11. Proposed second step of the oxidation of chlorinated phenols: epoxidation of 2,6-dichlorobenzoquinone.
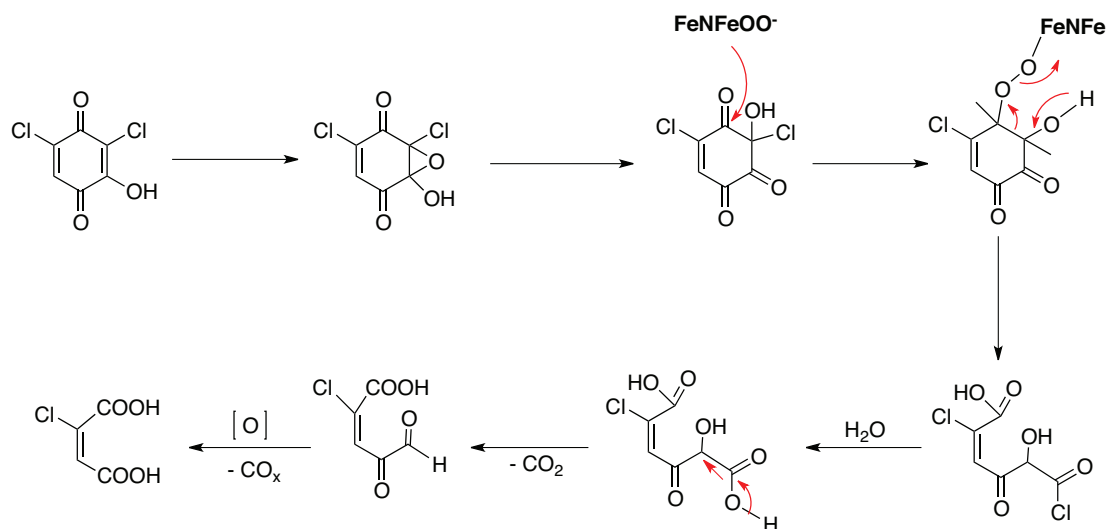
Scheme 12. Proposed mechanism of the cleavage of the aromatic cycle of chlorinated phenols.

The **14**-H_2O_2 catalytic system was more efficient than mononuclear FePcS-H_2O_2 system. The mechanistic studies show that the **14**-H_2O_2 system works via diiron-centered oxo and peroxo species, while monomeric FePcS was not active in the oxidation of chlorinated phenols in pure water.

4.6. Hydroacylation of olefins

μ-nitrido diiron complex **11** was used as an efficient catalyst for C–C bond formation reactions.[43] The complex **11** catalyzed the addition of acetaldehyde to unactivated cyclic or linear alkenes under inert atmosphere using low catalyst loading (0.01 mol %) in the absence of organic solvent. The **11**-^{t}BuOOH system was very efficient in the hydroacylation of olefins (Scheme 13).
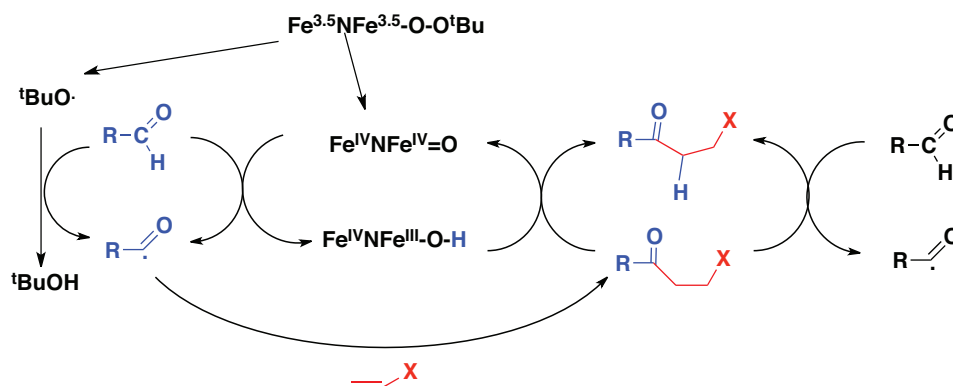
Scheme 13. Proposed mechanism for hydroacylation of olefins catalyzed by **11**.

The catalytic system was adapted for hydroacylation of cyclic and linear alkenes. In these reaction conditions, with octene-1 and 2-cyclohexen-1-one, only the formation of the anti-Markovnikov product was obtained. When allylbenzene and 2-propen-1-ol were used, anti-Markovnikov and Markovnikov products were obtained in 95/5 and 83/17 ratios. The allylbenzene, 2-allylphenol, and 2-cyclohexen-1-one can be easily oxidized in this method (Table 8). In all cases, neither benzylic nor allylic oxidation products were detected. An aromatic oxidation product was not observed in the oxidation of allylphenol.

Table 8. Hydroacylation of different olefins catalyzed by **11**.[a]

Entry	Substrate	Product	Conversion (%)	Selectivity (%)
1[b]			69	92
2[c]			86	52
3[d]			71	80
4			71	51
5			61	90
6			62	76

[a] Reaction conditions: olefin (10 mmol), acetaldehyde (100 mmol), tBuOOH (1.5 mmol, 70% aqueous solution), catalyst 1 (1 mmol, 0.01 mol%), high-pressure reactor, argon, 60 °C, 24 h. [b] 0.1 mol% catalyst loading. [c] Isolated mixture consisting of a 95/5 mixture of anti-Markovnikov and Markovnikov isomers. [d] Isolated mixture consisting of an 83/17 mixture of the isomers.

4.7. Oxidation of 2-mercaptoethanol

Oxidation of thiols is a significant biological and industrial process.[79−81] Two N-bridged diiron (IV) phthalocyanine cation radical complexes bearing Br and Cl were prepared and tested in oxidation of 2-mercaptoethanol[40] (Figure 12). The catalytic properties of **11-Br** were evaluated in the aerobic oxidation of 0.1 M solutions of 2-mercaptoethanol and 2-mercaptophenol in MeCN at 20 °C. Completely selective conversion of 2-mercaptoethanol to disulfide was observed after 5 h in the presence of 0.1 mol % of **11-Br**.
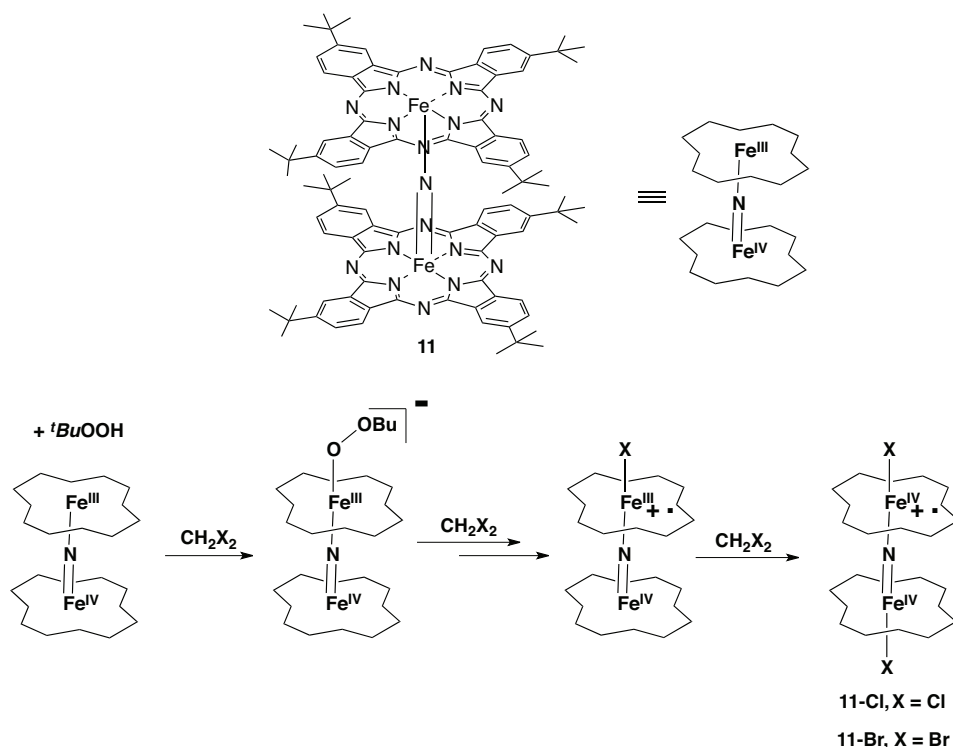
Figure 12. The formation of cation radical complexes of **11** bearing Br and Cl.

11-Br complex exhibited good catalytic activity in catalytic oxidation of thiols.

Complex **11** reacted with dicumyl peroxide to form a high-valent diiron complex that oxidized imidazole to unidentified products.[82]

The comparative study of the reactivity of **14** and corresponding μ-oxo diiron complex with sulfur-containing reductants (sodium dithionite, thiourea dioxide, sodium hydroxymethanesulfinate, and L-cysteine) showed a difference in reduction processes.[83]

The first DFT calculations showed a distinct difference in electronic structures between μ-oxo and μ-nitrido bridged diiron model complexes, which could explain the particular catalytic properties of μ-nitrido complex.[84]

5. Conclusions and outlook

Further development of the N-bridged diiron complexes can be achieved by their structural change. Appropriate variation in metals and macrocyclic ligands should allow the modification of their physico-chemical properties and, consequently, of catalytic properties. A large family of homo- and heterometallic complexes supported

by the same or different macrocyclic ligands in homoleptic or heteroleptic environment can be prepared. Phthalocyanine, porphyrin, porphyrazine, corrole, corrolazine, and other macrocyclic ligands in combination with Fe, Mn, Ru, Cr, etc. can be used. However, to access to certain structures, novel synthetic approaches should be developed.

Mononuclear and phthalocyanine and porphyrin metal complexes have been used for the construction of organized porous solids potentially useful in catalysis since these materials combine a high porosity and high concentration of active sites.[85,86]

The research on catalytic applications of μ-bridged bimetallic macrocyclic complexes is still in its infancy. It is expected that further synthetic and catalytic studies will be performed to access to various N-bridged bimetallic structures with modulated properties and, consequently, to increase the scope of catalytic reactions.

References

1. Eichhorn, H. *J. Porphyrins Phthalocyanines* **2000**, *4*, 88–102.

2. de la Torre, G.; Vázquez, P.; Agulló-López, F.; Torres, T. *Chem. Rev.* **2004**, *104*, 3723–3750.

3. de la Torre, G.; Claessens, C.; Torres, T. *Chem. Commun.* **2007**, 2000–2015.

4. Garcia, J.; Gonzalez, A.; Gouloumis, A.; Maya, E. M.; Perez, M. D.; Rey, B. D.; Vazquez, P.; Torres, T. *Turk. J. Chem.* **1998**, *22*, 23–31.

5. Liu, M. O.; Tai, C. H.; Sain, M. Z.; Hua, A. T.; Chou, F. *J. Photochem. Photobiol. A: Chem.* **2004**, *165*, 131–136.

6. de Saja, J. A.; Rodríguez-Méndez, M. L. *Adv. Coll. Interf. Sci.* **2005**, *116*, 1–11.

7. Costas, M. *Coord. Chem.* **2011**, *225*, 2912–2932.

8. Sorokin, A. B. *Chem. Rev.* **2013**, *113*, 8152–8191.

9. Sorokin, A. B.; Kudrik, E. V. *Catal. Today* **2011**, *159*, 37–46.

10. Aviv-Harel, I.; Gross, Z. *Chem. Eur. J.* **2009**, *15*, 8382–8394.

11. Goldberg, D. P. *Acc. Chem. Res.* **2007**, *40*, 626–634.

12. Rodriguez-Morgade, M. S.; Stuzhin, P. A. *J. Porphyrins Phthalocyanines* **2004**, *8*, 1129–1165.

13. Floris, B.; Donzello, M. P.; Ercolani. C. In *The Porphyrin Handbook Vol 18*; Kadish, K. M.; Smith, K. M.; Guilard, R., Eds. Elsevier Science: San Diego, CA, USA, 2003, pp. 1–62.

14. Summerville, D. A.; Cohen, I. A. *J. Am. Chem. Soc.* **1976**, *98*, 1747–1752.

15. Schick, G. A.; Findsen, E. W.; Bocian, D. F. *Inorg. Chem.* **1982**, *21*, 2885–2887.

16. Scheidt, R. W.; Summerville, D. A.; Cohen, A. I. *J. Am. Chem. Soc.* **1976**, *98*, 6623–6628.

17. Schick, G. A.; Bocian, D. F. *J. Am. Chem. Soc.* **1983**, *105*, 1830–1838.

18. Bocian, D. F.; Findsen, E. W.; Hofmann, J. A.; Schick, G. A.; English, D. R.; Hendrickson, D. N.; Suslick, K. S. *Inorg. Chem.* **1984**, *23*, 800–807.

19. Wagner, W. D.; Nakamoto, K. *J. Am. Chem. Soc.* **1988**, *110*, 4044–4045.

20. Li, M.; Shang, M.; Ehlinger, N.; Schulz, C. E.; Scheidt, W. R. *Inorg. Chem.* **2000**, *39*, 580–583.

21. Kudrik, E. V.; Afanasiev, P.; Alvarez, L. X.; Dubourdeaux, P.; Clemancey, M.; Latour, J. M.; Blondin, G.; Bouchu, D.; Albrieux, F.; Nefedov, S. E.; et al. *Nature Chem.* **2012**, *4*, 1024–1029.

22. Kadish, K. M.; Rhodes, R. K.; Bottomley, L. A.; Goff, H. M. *Inorg. Chem.* **1981**, *20*, 3195–3200.

23. Kudrik, E. V.; Albrieux, F.; Afanasiev, P.; Sorokin, A. B. *J. Porphyrins Phthalocyanines* **2013**, *17*, 791–798.

24. Li, M.; Scheidt. W. R. *J. Porphyrins Phthalocyanines* **2014**, *18*, 380–384.

25. Tong, C.; Bottomley, L. A. *Inorg. Chem.* **1996**, *35*, 5108–5109.

26. Stuzhin, P. A.; Hamdusha, M.; Homborg, H. *Mendeleev Commun.* **1997**, *7*, 196–198.

27. Ercolani, C.; Jubb, J.; Pennesi, G.; Russo, U.; Trigante, G. *Inorg. Chem.* **1995**, *34*, 2535–2541.

28. Ercolani, C.; Hewage, S.; Heucher, R.; Rowill. G. *Inorg. Chem.* **1993**, *32*, 2975–2977.

29. Donzello, M. P.; Ercolani, C.; Kadish, K. M.; Ou, Z.; Russo, U. *Inorg. Chem.* **1998**, *37*, 3682–3688.

30. Donzello, M. P.; Ercolani, C, Russo, U.; Chiesi-Villa, A.; Rizzoli, C. *Inorg. Chem.* **2001**, *40*, 2963–2967.

31. Goedkent, V. L.; Ercolani, C. *J. Chem. Soc., Chem. Commun.* **1984**, 378–379.

32. Bottomlev. L. A.; Gorce, J. N.; Goedken, V. L.; Ercolani, C. *Inorg. Chem.* **1985**, *24*, 3733–3737.

33. Kennedy, B. J.; Murray, K. S.; Homborg, H.; Kalz, W. *Inorg. Chim. Acta.* **1987**, *134*, 19–21.

34. Ercolani, C.; Gardini, M.; Pennesi, G.; Rossi, G.; Russo, U. *Inorg. Chem.* **1988**, *27*, 422–424.

35. Moubaraki, M.; Benlian. D.; Baldy, A.; Pierrot, M. *Acta Cryst. C.* **1989**, *45*, 393–394.

36. Rossi, G.; Gardini, M.; Pennesi, G.; Ercolani, C.; Goedken, V. L. *J. Chem. Soc. Dalton Trans.* **1989**, 193–195.

37. Sorokin, A. B.; Kudrik, E. V.; Bouchu, D. *Chem. Commun.* **2008**, 2562–2564.

38. Kudrik, E. V.; Sorokin, A. B. *Chem. Eur. J.* **2008**, *14*, 7123–7126.

39. Kudrik, E. V.; Afanasiev, P.; Bouchu, D.; Millet, J. M. M.; Sorokin, A. B. *J. Porphyrins Phthalocyanines* **2008**, *12*, 1078–1089.

40. Afanasiev, P.; Bouchu, D.; Kudrik, E. V.; Millet, J. M. M.; Sorokin, A. B. *Dalton Trans.* **2009**, 9828–9836.

41. Sorokin, A. B.; Kudrik, E. V.; Alvarez, L. X.; Afanasiev, P.; Millet, J. M. M.; Bouchu, D. *Catal. Today* **2010**, *157*, 149–154.

42. Kudrik, E. V.; Safonova, O.; Glatzel, P.; Swarbrick, J. C.; Alvarez, L. X.; Sorokin, A. B.; Afanasiev, P. *Appl. Catal. B.* **2012**, *113 − 114*, 43–51.

43. Alvarez, L. X.; Kudrik, E. V.; Sorokin, A. B. *Chem. Eur. J.* **2011**, *17*, 9298–9301.

44. Afanasiev, P.; Kudrik, E. V.; Millet, J. M. M.; Bouchu, D.; Sorokin, A. B. *Dalton Trans.* **2011**, *40*, 701–710.

45. Kudrik, E. V.; Sorokin, A. B. *Macroheterocycles* **2011**, *4*, 154–160.

46. Forde, M. M.; Grazia, B. C.; Armstrong, R.; Jenkins, R. L.; Ab Rahim, M. H.; Carley, A. F.; Dimitratos, N.; Lopez-Sanchez, J. A.; Taylor, S. H.; McKeown, N. B.; et al. *J. Catal.* **2012**, *290*, 177–185.

47. Kudrik, E. V.; Afanasiev, P.; Sorokin, A. B. *Macroheterocycles* **2010**, *3*, 19–22.

48. İşci, Ü.; Afanasiev, P.; Millet, J. M. M.; Kudrik, E. V.; Ahsen, V.; Sorokin, A. B. *Dalton Trans.* **2009**, 7410–7420.

49. İşci, Ü.; Dumoulin, F.; Ahsen, V.; Sorokin, A. B. *J. Porphyrins Phthalocyanines* **2010**, *14*, 324–334.

50. Stuzhin, P. A.; Ivanova, S. S.; Dereven'kov, I.; Makarov, S. V.; Silaghi- Dumitresku, R.; Homborg, H. *Macroheterocycles* **2012**, *5*, 175–177.

51. Kudrik, E. V.; Afanasiev, P.; Bouchu, D.; Sorokin, A. B. *J. Porphyrins Phthalocyanines* **2011**, *15*, 583–591.

52. İşci, Ü. *J. Porphyrins Phthalocyanines* **2013**, *17*, 1022–1026.

53. Schröder, D. *Acc. Chem. Res.* **2012**, *45*, 1521–1532.

54. Pratt, I.; Mathieson, J. S.; Güell, M.; Ribas, X.; Luis, J. M.; Cronin, L.; Costas, M. *Nature Chem.* **2011**, *3*, 788–793.

55. Afanasiev, P.; Kudrik, E. V.; Albrieux, F.; Briois V.; Koifman, O. I.; Sorokin, A. B. *Chem. Commun.* **2012**, *48*, 6088–6090.

56. Bernadou, J.; Meunier, B. *Chem. Commun.* **1998**, 2167–2173.

57. Balahura, R. J.; Sorokin, A.; Bernadou, J.; Meunier, B. *Inorg. Chem.* **1997**, *36*, 3488–3492.

58. Kienast A.; Homborg, H. *Z. Anorg. Allg. Chem.* **1998**, *624*, 233–238.

59. English, D. R.; Hendrickson, D. N.; Suslick, K. S. *Inorg. Chem.* **1985**, *24*, 121–122.

60. De Groot, F. *Chem. Rev.* **2001**, *101*, 1779–1808.

61. Glatzel, P.; Bergmann, U. *Coord. Chem. Rev.* **2005**, *249*, 65–95.

62. Westre, T. E.; Kennepohl, P.; DeWitt, J. G.; Hedman, B.; Hodgson, K. O.; Solomon, E. I. *J. Am. Chem. Soc.* **1997**, *119*, 6297–6314.

63. Ough, E.; Gazina, Z.; Stillman, M. J. *Inorg. Chem.* **1991**, *30*, 2301–2310.

64. Nyokong, T.; Gazina, Z.; Stillman, M. J. *Inorg. Chem.* **1987**, *26*, 548–553.

65. Pergrale, C.; Sorokin, A. B. *C. R. Chimie* **2000**, *3*, 803–810.

66. Pérollier, C.; Pergrale-Mejean, C.; Sorokin, A. B. *New J. Chem.* **2005**, *29*, 1400–1403.

67. Beyrhouty, M.; Sorokin A. B.; Daniele, S.; Hubert-Pfalzgraf, L. G. *New J. Chem.* **2005**, *29*, 1245–1248.

68. Geraskin, I. M.; Pavlova, O.; Neu, H. M.; Yusupov, M. S.; Nemykin, V. N.; Zhdankin, V. V. *Adv. Synth. Cat.* **2009**, *351*, 733–737.

69. Neu, H. M.; Zhdankin, V. V.; Nemykin, V. N. *Tetrahedron Lett.* **2010**, *51*, 6545–6548.

70. Holmen, A. *Catal. Today* **2009**, *142*, 2–8.

71. Olivier, L.; Haag, S.; Mirodatos, C.; van Veen, A. C. *Catal. Today* **2009**, *142*, 34–41.

72. Vora, B.; Chen, J. Q.; Bozzano, A.; Glover, B.; Barger, P. *Catal. Today* **2009**, *141*, 77–83.

73. Shilov, A. E.; Shul'pin, G. B. *Chem. Rev.* **1997**, *97*, 2879–2932.

74. Periana, R. A.; Taube, D. J.; Gamble, S.; Taube, H.; Satoh, T.; Fujii, H. *Science* **1998**, *280*, 560–564.

75. Punniyamurthy, T.; Velusamy S.; Iqbal, J. *Chem. Rev.* **2005**, *105*, 2329–2363.

76. Llabresi Xamena, F. X.; Casanova, O.; Tailleur, R. G.; Garcia, H.; Corma, A. *J. Catal.* **2008**, *255*, 220–227.

77. Kockrick, E.; Lescouet, T.; Kudrik, E. V.; Sorokin, A. B.; Farrusseng, D. *Chem. Commun.* **2011**, *47*, 1562–1564.

78. Colomban, C.; Kudrik, E. V.; Pavel Afanasiev, P.; Sorokin, A. B. *Catal. Today* **2014**, *235*, 14–19.

79. Basu, B.; Satapathy, S.; Bhatnagar, A. K. *Catal. Rev. Sci. Eng.* **1993**, *35*, 571–609.

80. Shirai, H.; Tsuiki, H.; Masuda, E.; Koyama, T.; Hanabusa, K.; Kobayashi, N. *J. Phys. Chem.* **1991**, *95*, 417–423.

81. Chauhan, S. M. S.; Kumar, A.; Srinivas, K. A. *Chem. Commun.* **2003**, 2348–2349.

82. Zaitseva, S. V.; Simonova, O. R.; Zdanovich, S. A.; Kudrik, E. V.; Koifman, O. I. *Macroheterocycles* **2014**, *7*, 55–59.

83. Dereven'kov, I. A.; Ivanova, S. S.; Kudrik, E. V.; Makarov, S. V.; Makarova, A. S.; Stuzhin, P. A. *J. Serb. Chem. Soc.* **2013**, *78*, 1513–1530.

84. Silaghi-Dumitrescu, R.; Makarov, S. V.; Uta, M. M.; Dereven'kov, I. A.; Stuzhin, P. A. *New J. Chem.* **2011**, *35*, 1140–1145.

85. Zhao, M.; Ou, S.; Wu, C. D. *Acc. Chem. Res.* **2014**, *47*, 1199–1207.

86. Gu, Z. Y.; Park, J.; Raiff, A.; Wei, Z.; Zhou, H. C. *ChemCatChem.* **2014**, *6*, 67–75.